RSC Advances

ROYAL SOCIETY OF CHEMISTRY

www.rsc.org/advances

Investigation on synthesis, crystal structure and third-order NLO properties of a new stilbazolium derivative crystal: A promising material for nonlinear optical devices

K.Senthil[a], S.Kalainathan[a]*, A.Ruban Kumar[a], P. G. Aravindan[b]

[a, a*] Centre for Crystal Growth, School of Advanced sciences, VIT University, Vellore - 632 014, Tamilnadu, India.

[b] Crystal Growth and Crystallography Division, School of Advanced Sciences, VIT University, Vellore 632 014, India.

Corresponding author: Phone: +91-416-2202350 Fax: 0416-2243092

E-mail Address: kalainathan@yahoo.com

Abstract

A new organic stilbazolium derivative crystal 2-[2-(3-hydroxy-4-methoxy-phenyl)-vinyl]-1-methyl-pyridinium naphthalene-2-sulfonate dehydrate ($C_{25}H_{23}NO_5S.2H_2O$) (VSNS) has been successfully synthesized. Single crystals were grown in a mixed solvent of methanol: acetonitrile (1:1) by using a slow evaporation method at room temperature. Solubility of the synthesized VSNS material was experimentally determined for various temperatures using methanol/acetonitrile mixed solvent. A single crystal x-ray diffraction study confirms the crystal structure and morphology of VSNS. The crystalline nature of title material was analyzed by powder x-ray diffraction analysis. The presence of expected functional groups and molecular structure of VSNS was identified by FT-IR and ^1H NMR spectroscopic studies. The optical absorption of VSNS has been recorded using UV-Vis-NIR spectral analysis, and its linear optical constants such as the absorption coefficient, band gap, extinction coefficient, refractive index and reflectance have been calculated. The luminescence property of the grown crystal shows the green emission radiation. The thermal stability of grown crystal has been analyzed by TG/DTA studies. The hardness, Meyer index, yield strength, and elastic stiffness constant were estimated for the grown crystal using Vickers microhardness tester. Layer growth pattern was observed in chemical etching studies by Carl Zeiss optical microscope with a 50x magnification. Laser damage

threshold energy has been measured by using Nd: YAG laser (1064 nm). The variation of the dielectric response of the grown crystal has been studied at room temperatures. The third order nonlinear optical property of VSNS was investigated in detail by Z-scan technique using He-Ne laser at 632.8nm. The second-order molecular hyperpolarizability γ of the grown crystal is 7.986 $x10^{-34}$ esu. The encouraging result of the Z-scan studies confirms that the VSNS crystal might be a possible candidate material for the photonics device, optical switches, and optical power limiting applications.

1. Introduction

In the 21st century, nonlinear optical (NLO) optical materials are a new frontier of science and development of new technologies of photonics.[1,2] These materials are influence potential applications such as information processing, optical computing,[3] telecommunication,[4-6] 3D optical data storage,[7,8] lasers and optical power limiting.[9] Therefore, the synthesis of new organic compounds with large nonlinear optical properties has attracted the interest of many research groups, which are the primary interest in the possibilities for reversibly switching NLO systems.[10,11] Compared with inorganic materials; organic materials have attracted much research interest recently because of their potential properties like short response time, a small dialectic constant and large electro-optic (EO) coefficient.[12] Organic single crystals have delocalized π- electrons with conjugated double bond systems. Hence, they are increasing the most interest over the several years because of their source of fast and large macroscopic nonlinearities, high optical quality, superior long-term orientational, high packing densities, and larger photochemical stabilities.[13, 14] Effective NLO organic materials contain suitable electron donor and electron acceptor groups through π- conjugated electronic bridge flank either end of the system.[15] In particular, the strong delocalization of π- electrons causes the large molecular hyperpolarizability and the nonlinear

susceptibility in the organic molecule can lead to a significant enhancement of the third-order nonlinear optical properties of the materials.

For the past few years, the third-order nonlinear optical materials have attracted because of their application in ultrafast optical switching and devices.[16] Among the various clauses of techniques developed by theoretically and experimentally in the worldwide for the measurement of NLO properties. Z- Scan technique is a simple and effective experimental method to measure the intensity dependence of the third-order optical nonlinearities of the materials.[17, 18] It is capable of measure the information not only on the sign and magnitude but also on the real (nonlinear refraction) and imaginary part (nonlinear absorption) of the material. The high ratio of real and imaginary part of the third-order nonlinear optical susceptibility is essential for effective optical switching applications.[19]

In this paper, we report the synthesis, growth of a new VSNS crystal from stilbazolium family. The grown crystals were characterized by different instrumentation technique in order to check its suitability for device fabrications. Its crystal structure has been confirmed by single crystal x- ray diffraction studies. The grown crystals were also systematically characterized by X-ray powder diffraction, and Fourier transform infrared, Nuclear magnetic resonance, optical, luminescence, thermal properties, mechanical behaviour, laser damage threshold dielectric and chemical etching studies. In the last section, the detailed study of third order nonlinear optical properties of grown crystal was investigated by using the Z- scan technique are discussed and reported.

2. Experimental Procedures

2.1. Material Synthesis

All high-purity commercially available reagents in Scheme 1 were purchased and used without further purification. VSNS was synthesized via two-step synthesis route. In the first step, 2-[2-(3-hydroxy-4-methoxyphenyl)-vinyl]-1-methyl-pyridinium iodide (A) was

synthesized (condensation reaction method) by mixing stoichiometry ratio of 1, 2-dimethyl pyridinium iodide, isovanillin in hot methanol and piperidine (few drops) was added as a catalyst. The resulting mixture solution was refluxed for 10 hr to form a yellow salt. The resultant A was filtered off and washed with diethyl ether to remove the unreactant material and purified by recrystallization in methanol. Then, in the second step VSNS was synthesized by counter-anion exchange reaction of A with sodium 2- naphthalene sulfonate as shown in scheme 1. The resulting material (A) was dissolved in deionized water (40ml) and treated with a saturated solution of sodium 2-naphthalene sulfonate and further heated for 1 h at 80°C. The precipitate appeared when the solution was cooled to ambient temperature and was isolated by filtration and dried. The purity of the title salt was increased by three times successively recrystallization using methanol solution.

2.2. Solubility, crystal growth and morphology

The solubility study is one of the important parameters which decide to achieve desired concentration of material, growth method and the growth rate of crystal and which is depends on its temperature. Thermodynamically this means that, in a saturated solution the chemical potential of the pure solid is equal to the chemical potential of the same solute.[20] The solubility of VSNS using purified salt was measured by dissolving the solute in 100 ml of mixed solvent of methanol: acetonitrile (1:1) for different temperature in the range 30-45ºC with 5 ºC interval. The solubility study has been carried out in a ultra-cryostat bath with a control accuracy of ±0.01 ºC. Initially, the cryostat was maintained at 30 ºC and continuously stirred with a motorized magnetic stirrer. The purified salt was added step by step to 100ml of methanol: acetonitrile mixed solvent in an airtight container on the bath until attaining supersaturation. The equilibrium concentration of the supernatant liquid of the solute was estimated by gravimetrically. In this experiment, the masses of the solvent and solute were weighed using an analytical balance (accuracy ± 0.0001 g). In the same manner was repeated

to estimate the equilibrium concentration of the amount solute dissolved in 100 ml at 30- 45 ºC. The solubility curve of VSNS at different temperature exhibits good solubility in methanol: acetonitrile mixed solvent and is presented in Fig.1. It was observed that solubility of VSNS increases dramatically with an increase of temperature.

The saturated solution of the purified salt of VSNS at 40°C was prepared by using the mixed solvent of methanol: acetonitrile (1:1) according to the determined solubility data. The prepared solution was filtered and transferred to 150ml beaker, and it was tightly covered with aluminum foil to control the rate of evaporation of the solvent. Then the beaker was kept in a constant temperature water bath at 40°C. Crystallization was allowed by the temperature of the bath by reducing the temperature at a rate of 0.20/day. After 35 days, good quality single crystals of VSNS with dimensions 7 x 4 x 2.5mm^3 were obtained. The photograph of as-grown crystals of VSNS is shown in Fig.2. The morphology of VSNS was indexed by WinXMorph software program using a single crystal XRD data (cif format) was used as input.[21] The indexed morphology of VSNS is shown in Fig. 3. It was found that growth rate of VSNS elongated along with crystallographic b-axis compared to other two growth directions.

3. Results and Discussion

3.1. Powder X-ray diffraction and Single crystal studies

The fine powder of grown crystal is subjected to BRUKER X-Ray diffractometer with the CuKa radiation (λ=1.540598 Å) in order to demonstrate the crystalline nature and purity. The sample recorded over the range 10–60° at the scanning rate of 0.02◦ S^{-1} (2θ) at room temperature. The various planes of reflection at specific 2θ angles were indexed using Powder X program. The experimentally observed XRD peaks are in good agreement with the single crystal XRD pattern based on the single crystal structure of VSNS as shown in Fig. 4. The appearances of well-defined sharp Bragg's peaks at specific 2θ angles confirm good crystalline property of the grown VSNS crystal.

Suitable crystal of VSNS was subjected to single crystal X-ray structure studies using Bruker Kappa APEX II diffractometer with MoKα (λ=0.71073Å) radiation. The grown crystal structure was solved by direct methods using SHELXS-97 and refined by full-matrix least squares against F_2 using SHELXL-97 software programe.[22] It is observed that the compound crystallized in centrosymmetric space group P21/n consist of cation and anion with monoclinic crystal system and R factor equal to 0.0331. The ORTEP view of VSNS was shown in Fig. 5. The crystal data summary is given in the Table .1. The maximum deviation from the plane of cation and anion molecule appears at C3 [0.101(2) Å] and C22 [-0.005(2) Å and N1 [0.0358(2) Å, respectively. It is clearly shown in VSNS structure that two planes of anion and cations are near to perpendicular with 83.8(1)˚. The torsion angle value at C5-C6-C7-C8=178.89(15)˚ shows that the phenyl group adopted trans conformation. There is a short contact exist between H4 and H7 due to the trans conformation and increase in bond angle from the standard value at C5 and C1 [C4-C5-C6 = 123.91(15)˚]. The methoxy group [O2=-0.0128(1) & C15=0.059(3)] slightly deviated from the mean plane of ring atoms are C8, C9, C10, C11, C12 & C13 in VSNS.

In the crystal packing of VSNS predominantly stabilized by O-H…O and C-H…O hydrogen bonds and aromatic interactions. There is a network chain associated with water molecules and the neighbour asymmetric residue unit running through ‘AC ‘plane axis. It is also noted that O-H...O networks are involved in translational units along b-axis through donor and acceptor atoms of O1…O7*…O6**…O3*** (indicated stars are translational units). The potential hydrogen bonds that sustain the structure of VSNS are listed the Table 2. Selected bond lengths and angles of VSNS are given in Tables 3. There are well-defined π - π interactions between symmetry generated pairs of the entities involved in the crystal packing. Particularly H12 of C12 forming π - interaction with centroid of other ring systems of C16-

C17-C23 and C24-C25 with an angle of 151.7˚. A three-dimensional view of the molecular packing diagram of VSNS is shown in Fig. 6.

3.2. FT-IR Spectral Studies

The vibrational spectral analysis of VSNS was recorded to confirm the various modes of functional groups present in the grown crystals by using SHIMADZU IRAFFINITY spectrometer and in the scan region 4000–400 cm^{-1} as shown in Fig. 7. The absorption band at 3375 and 3255 cm^{-1} are due the O-H stretching vibrations on isovanillin and presence of a water molecule in the title compound. The aromatic C-H stretching mode observed at 3062 cm^{-1} in the spectrum. The absorption peak obtained at 2956, and 2835 cm^{-1} is due to the alkyl C-H stretching vibrations. The aromatic ring C=C stretching vibrations is assigned to peaks at 1618 cm^{-1}, 1566 cm^{-1} and 1502 cm^{-1} respectively. The in-plane O-H group deformation vibrations in isovaniline ring reported near 1257 and 1436 cm^{-1}.[23] The peak at 1388 cm^{-1} is assigned to the C-N stretching and CH_2 bending vibrations. The stretching frequency of S=O at 1178 cm^{-1}clearly indicate that the presence of SO_3 group in the crystal lattice. The absorption band at 1031 cm^{-1} establishes formation of the title compound by C-H olefin bond. The presence of methoxy (O-CH_3) group gives its stretching mode in the region 1000-1100 cm^{-1}. The very week intensity band observed at 972 cm^{-1} is due to the C-H deformation mode of the title molecule.[24] Thus, the assignments of the various absorption frequencies confirm the formation of VSNS crystal.

3.3. ^{1}H NMR Spectral Studies

NMR spectroscopy is considered as the most useful analytical techniques for determining the structure and the nature of the immediate environment of each molecule. The experiments were performed on a BRUKER instrument operating with 400 MHz spectrometer. Fig. 8 shows the ^{1}H NMR spectra of the title compound in DMSO-d_6 shows a quintet chemical shift at 2.540 ppm. Also, the chemical shift of a water molecule in DMSO-d_6 it gives chemical

shift at 3.423ppm. A methyl proton attached with pyridine ring (N-CH_3) gives a singlet peak at 4.363 ppm. Protons of the methyl group in aldehyde ring (O-CH_3) shows a singlet peak at 3.882ppm. Two doublet's chemical shift observed at 7.076 ppm, and 7.751ppm are due to the two olefin hydrogen's (HC=CH). The pyridinium ring gives two doublets peak at 8.444ppm, and 8.865ppm are corresponding to the third and six places of hydrogen's (C-H), it is the neighbor of (N-CH_3) bond. Also, it produces one triplet peak at 8.483ppm, and one doublet at 7.772ppm is due to the fourth and fifth position hydrogen's. Aromatic protons of second and six places showed multiplet peaks in the range from 7.300 ppm to 7.394ppm. Three multiplet peaks were observed at 7.550ppm, 7.858ppm and 7.934ppm are due to the ring hydrogen's of naphthalene. The singlet chemical shift at 8.194 ppm was assigned to first place hydrogen of the naphthalene. Proton of the hydroxyl group shows a singlet peak at 9.343ppm. Thus, the observed chemical shift establishes the molecular structure of the title compound.

3.4. UV Vis NIR Spectral Analysis

The optical transmittance study is a very useful to identify the optical transmission range and cut-off wavelength of the crystal. Also, it is very useful to understand about its electronic transition states, when interaction of light with a molecule. The optical absorption spectrum of VSNS was recorded in the wavelength range 190 nm to 1100nm with a crystal of thickness 1mm by using ELICO SL 218 double beam UV-Vis–NIR spectrometer. From the absorption spectrum (Fig. 9), it is revealed that the absence of transmission of light in the UV region is can be the absorption of UV light involves the strong electronic transitions electrons from the ground state to excited state (higher energy states). The optical cutoff wavelength of the VSNS crystal is found to be 390 nm, and the crystals have the good optical transmittance percentage between 390 nm to 1100 nm (Vis-NIR region). For the optoelectronic and NLO applications the crystal must be good transparent in the Vis-NIR region.[25] The lower cut-off wavelength of the grown crystal is due to the π-π^* orbital electronic transitions through the

stilbazolium chromophore. The band gap energy at cut-off wavelength was calculated using the relation

$$E_g = hc / \lambda_{max}(nm) \quad (1)$$

where h is the Planck constant, c is the velocity of light and λ is the cut-off wavelength of the crystal. Hence, the calculated value of band-gap energy of the grown crystal was found to be 3.17 eV.

Determination of energy band gap, extinction coefficient and refractive index

The optical absorption coefficient (α) was determined using the following formula,

$$\alpha = \frac{2.303\log\left(\frac{1}{T}\right)}{t} \quad (2)$$

where T is the transmittance and t is the thickness of the crystal. As a direct band gap (E_g) has been determined from the transmission spectra and the optical absorption coefficient of the crystal (α) near the absorption edge is given by the following relation

$$\alpha = \frac{A(h\nu - E_g)^{1/2}}{h\nu} \quad (3)$$

where A is a constant, E_g the optical band gap of the crystal, h the plank's constant and υ is the frequency of incident photons. The plot of transmittance and reflectance for VSNS is shown in Fig. 10a. The band gap of VSNS crystal was estimated by plotting $(\alpha h\upsilon)^2$ against the photon energy (hυ) (Tauc's plot) as shown in Fig.10b. The band gap energy (E_g) of the grown crystal was estimated by exploring a straight line in the linear region near the onset of the absorption edge to the energy axis $(\alpha h\upsilon)^2=0$. From Fig.10b, the estimated band gap energy was found to be 3.252 eV. As a result of wide band gap of the VSNS crystal confirms

the large transmittance window in the visible region.[26] The extinction coefficient (K) can be obtained from the following relation

$$K = \frac{\lambda\alpha}{4\pi} \tag{4}$$

The plot of extinction coefficient (K) as a function of wavelength is shown in Fig. 10c. From the graph, it is observed that extinction coefficient (K) value increases with an increase in the photon energy.

The transmittance (T) is given by

$$T = \frac{(1-R)^2 \exp(-\alpha t)}{1-R^2 \exp(-2\alpha t)} \tag{5}$$

The reflectance (R) in terms of the absorption coefficient can be derived from the following relation

$$R = \frac{\exp(-\alpha t) \pm \sqrt{\exp(-\alpha t)T - \exp(-3\alpha t)T + \exp(-2\alpha t)T^2}}{\exp(-\alpha t) + \exp(-2\alpha t)T} \tag{6}$$

It is observed that reflectance (R) increases with an increase in the photon energy and is shown in Fig.10a.

$$n_0 = -(R+1) \pm 2\frac{\sqrt{R}}{(R-1)} \tag{7}$$

The linear refractive index (n_0) of the crystal was determined in the terms of reflectance (R) using the relation. The linear refractive index (n_0) the grown crystal is found to be n_0=0.9284 at 1100nm and it can be used to calculate the third nonlinear optical susceptibility of the material. Fig.10d shows the variation refractive index (n_0) as a function of photon energy for VSNS crystals. The optical studies revealed that, VSNS crystal possesses good optical behaviour for using it in device applications.

Thus, the extinction coefficient (K) and refractive index (n_0) are depending on the wavelength. It is understood that the higher value of photon energy will enhance the optical efficiency of the material.

3.5. Luminescence studies

In general photoluminescence (PL) in solids, the molecules are excited by external energy from a light source, and the excitation state is released as luminescence light.[27] In order to identify the nature of emission band of VSNS, the excitation spectrum was recorded using a using F-7000 FL Spectrophotometer in the range of 400-750 nm at room temperature. The emission spectrum of the sample was recorded in the range 450-750nm with the excitation wavelength of sample at 390nm is shown in Fig. 11. From the emission spectrum, title compound exhibits a strong and broad emission peak at 553nm which is related to the π-π* localized electron between the donor and acceptor groups through stilbazolium chromophore (π-conjugated double bond), which lead to its luminescence characteristic nature. Thus, this result indicates that the VSNS crystal has stronger photon energy absorption band in UV region at 390nm and a weaker green emission radiation at 553nm, which is revealed to its high purity with a high degree of crystallinity of VSNS crystals.[28] It indicates that the defect free, good crystallinity are useful optoelectronic device applications.

3.6. Thermo-gravimetric and Differential Thermal Analysis

To study the phase transition, melting point and various stages of decomposition point of the crystal system, the thermogravimetric (TG) and differential thermal analysis (DTA) of grown crystal have been carried out in the temperature range 35-550^{o}C by using Netzsch STA-449F3 analyzer equipment in the N_2 atmosphere. The initial mass of the powder sample of VSNS was 4.340 mg was used for the analysis. The obtained TG/DTA curve of the title

compound is shown in Fig. 12. From the TGA curve, it is noticed that there is no weight loss and phase transition between the 35 -196.6^{o}C, and it is evident that the title compound is very stable up to 196.6 ^{o}C. The title compound starts to decompose with three different stages, during the first stage is a weight loss of 3.56% of the initial mass commences between 196.6 – 321.6 ^{o}C due to dehydration of water molecules and volatile substances. During the next stage, the maximum decomposition with the weight loss 60.74% start at 321.6 ^{o}C and a temperature beyond 387.5 ^{o}C and again weight losses occur between 387.5 ^{o}C -549.7 ^{o}C and it has concluded that the complete decomposition of the title compound. In the DTA trace, the endothermic peak at 204.3 ^{o}C which represents the melting point of VSNS crystal and it is followed by the rapid decomposition in DTA peak at 371.6 ^{o}C is due to the complete composition of VSNS crystal as gaseous stage that is coincides with the maximum weight losses in TG curve. The residual mass of the title compound is 15.19% charred as carbon at 549.9 ^{o}C. Thus, the TG/DTA studies establish its suitability to laser experiments application of this crystal is texture to 196.6 ^{o}C.

3.7. Microhardness Studies

Measurement of microhardness testing is a useful method for to calculate the mechanical properties of the materials such as hardness number, fracture behaviour, elastic stiffness constant, yield strength and plasticity.[29- 31] A hardness properties of the material primarily depends on the crystal structure.[32] Mechanical stability of the material plays an essential role in the fabrication of devices. The hardness measurements of VSNS crystal were made on the well-defined prominent plane (1 0 0) using MH-112 Vicker's hardness tester fitted with a pyramid indenter. In the present study, the indentation time of 10s was used for all indentations for all loads ranging from 10-100 g. The Vickers hardness value of each load has calculated using the expression

$$Hv=1.8544P/d^2 \ Kg/mm^2 \quad (8)$$

where, P is the load applied in kilogram (kg) and d is the average diagonal length of the indentation impression in μm. A plot drawn between the loads and the corresponding hardness number was depicted in Fig. 13. It is showed that the hardness number increases with the increase of applied load, which refers to the crystal exhibits reverse indentation size effect (RISE) behavior.[33] The relation between load P and average indentation d is given by using Meyer's law [34] and depicted in Fig. 14a, gives a straight line. The estimated value of Mayer's index (n) determines the work hardening coefficient for VSNS crystal and is equal to 2.70, which concluded that grown crystal falls under the soft material category, which is good agreement with the reverse indentation size effect (RISE).[35] From the Meyer index value n>2, the yield strength σ_y of the crystal has been using the expression

$$\sigma_y = \frac{H_v}{2.9}[1-(n-2)]\left(\frac{12.5(n-2)}{1-(n-2)}\right)^{n-2} \quad (9)$$

A plot of load dependent yield strength σ_y is shown in Fig. 14b. Also, the elastic stiffness constant has been calculated using Wooster's empirical relation.[36]

$$C_{11} = (Hv)^{7/4} \quad (10)$$

The elastic stiffness constant (C11) gives an idea about strength and nature of bonding of atoms to its neighbor. Fig. 14c shows the plot between load and stiffness constant for the title compound. The calculated Vicker's hardness values, stiffness constant and yield strength σ_y values of VSNS crystal for different loads from 10 - 100 g are given in Table 4. According to the Hays and Kendall's approach [37], non-linear behavior of hardness material can be analytically explained by using the expression $P = W+A_1d^2$, where W is the minimum load to initiate plastic (permanent) deformation in g, A_1 is the load-independent constant. The values of W and A_1 have been estimated from the plots drawn between the experimental data as P versus d^2 shown in Fig. 14d. The estimated negative value of W reveals that the grown VSNS

crystals are exhibiting behavior of reverse ISE.[38] The corrected hardness H_o value (Table 5) of VSNS crystal has been calculated by using the relation:

$$H_o = 1854.4\ A_1 \quad (11)$$

Thus, the hardness study of VSNS crystal has sufficient mechanical strength for various nonlinear device fabrications.

3.8. Chemical Etching Studies

Etching of surface is a very simple and powerful characteristic to analyze the quality of the grown crystal and also gives structural defects and crystal growth mechanism. The NLO applications of grown crystal primarily depend on high-quality single crystals because of defect configuration occur during the crystal growth which cause in the distortion of efficiency of the optical beam in the laser material processing. Hence, it is necessary to analyze the microstructural imperfections present in the grown crystals.[39] In the present investigation, the etching studies of VSNS crystal were carried out using by methanol as etchant at room temperature at different durations 10s, 20s and 40s. After the crystal had etched with methanol, the etched surfaces were dried by using tissue paper and their etched pattern was examined by using Carl Zeiss optical microscope with a 50x magnification. Fig.15a shows the before etching pattern of as grown VSNS crystal and after etching it produces rectangular well-defined etch pits for 20s is shown Fig.15b. There was no morphology of the etch pits change with an increase of etching time which suggesting that the grown crystal has good optical quality with less dislocations shown in Fig15 c(40s).

3.9. Laser-Induced Damage Threshold Studies

The laser damage threshold of optical crystal caused by various physical processes such as electron avalanche, multiphoton absorption and photoionization for the transparent materials whereas in the case of high absorbing materials, the damage threshold is mainly due to the

temperature rise, which leads to strain induced fracture.[40,41] The utility of NLO crystal depends not only on the linear and nonlinear optical properties but also largely on its surface quality to ability to withstand high power intensities.[42] In the present study, the laser damage threshold study of grown VSNS crystal have been measured using a Q-switched pulsed Nd: YAG (1064 nm) laser with operating in transverse mode (TM_{00}) and pulse width of 10 ns in the frequency rate of 10 Hz. Laser beam of diameter 1mm was used to irradiating the crystal surface. The output of the incident laser beam was controlled with a variable attenuator and delivered to onto the crystal that was placed at the focus of the converging lens of focal length 30 cm. The energy density of the input laser beam was measured by using a power meter (model no: EPM 2000) at which the crystal was damaged.

The energy density has been calculated using the expression

$$\text{Power density } (P_d) = E / \tau\pi r$$

Where E is the input energy density (mJ), τ is the pulse width (ns) and r is the area of the circular spot (mm). The calculated value of laser damage threshold value of VSNS was found to be 1.94 GW/cm^2, which is higher than KDP (0.20) and urea (1.50) crystals.[43] Hence, the grown crystal has good surface because of its high laser damage threshold value. Thus, the title crystal is useful for high power laser applications.

3.10. Dielectric studies

3.10.1. Dielectric constant and dielectric loss measurements

Dielectric measurements have been useful to provide information about electro-optical molecular responses, molecular anisotropy, structural changes and transport phenomena within the crystalline materials.[44- 45] The dielectric constant and loss of the grown crystal has been carried out as a function of frequency various from 50Hz to 5 MHz at room temperature

by using HIOKI 3532-50 LCR HITESTER meter. The as-grown optical quality single crystals 2mm thickness with 1 0 0 face of VSNS was used for studying of both dielectric constant and dielectric loss measurement. The sample surfaces were coated by silver paste to make uniform electrical contact with the surface of electrodes. The sample cell was placed in a thermal insulation container in which the electric heater was housed for ensuring good thermal conditions of the cell. The dielectric constant (ε_∞) of VSNS was calculated using the following equation,

$$\varepsilon_\infty = Ct/ \varepsilon_o A \quad (12)$$

where C is the capacitance, t is the crystal thickness, ε_o is the vacuum dielectric constant, and A is the area of the crystal. Fig.16 shows the variations of dielectric constant vs. log frequency. From the Fig .16, the values of dielectric constant are high in the lower frequency region and further the dielectric constant decreases with increase in frequencies. The higher value of dielectric constant at low frequencies (5Hz) is due to the contribution of all the four polarizations namely, space charge, orientational, electronic and ionic polarization. The low value at higher frequency region is may be due to the inability of the dipoles to comply with the external field.[47, 48] Fig.17 represents the variation of dielectric loss as a function of log frequency. It is found that from the graph, the values of dielectric loss are decreases with increase in frequencies. Thus, the characteristic very low values of dielectric constant and dielectric loss at high frequencies for these crystals suggests that the enhanced optical quality with lesser defects. This indicates that the crystal can be useful for optoelectronic applications and NLO devices.[49]

3.10.2. Solid state parameters of VSNS crystal based on single crystal XRD

The dielectric constant at high frequency is explicitly dependent on the valence electron of compound, Plasma energy, Penn gap and the Fermi energy. The Penn gap is calculated by fitting the dielectric constant with the Plasmon energy.[50] From the empirical formula, the

formula weight of the grown crystal is 485.54g/mol^{-1}, and the total number of the valence electron (Z) in the structural unit is Z=180. The density of the title compound was found to be, ρ 1.390 mg/m^3.From the dielectric constant (ε_∞), the dielectric constant at 1MHz was calculated to be 716. From these data, the valence electron plasma energy (ħωp), given by Jackson et al.[51]

$$\hbar\omega_p = 28.8\left(\frac{Z_\rho}{M}\right)^{\frac{1}{2}} \tag{13}$$

Explicitly ħωp dependent Penn gap (Ep) and the Fermi energy (E_F) in eV are derived from the following relations [49] and is given by

$$E_p = \frac{h\omega_p}{(\varepsilon_\infty - 1)^{1/2}} \tag{14}$$

$$E_F = 0.2948(\hbar\omega_p)^{1/2} \tag{15}$$

The electronic polarizability (α) of the title crystal can be calculated using the relation [52],

$$\alpha = \left[\frac{(\hbar\omega_p)^2 S_0}{(\hbar\omega_p)^2 S_0 + 3E_p^{\,2}}\right] \times \frac{M}{\rho} \times 0.396 \times 10^{-24} cm^3 \tag{16}$$

where S_0 is a constant for a particular material which is obtained by using the relation

$$S_0 = 1 - \left[\frac{E_p}{4E_F}\right] + \frac{1}{3}\left[\frac{E_p}{4E_F}\right]^2 \tag{17}$$

The value of electronic polarizability α is also be confirmed by using the Clausius-Mossotti relation, which is agrees with that of values obtained from equation 16.

$$\alpha = \frac{3M}{4\pi N_a \rho}\left(\frac{\varepsilon_\infty - 1}{\varepsilon_\infty + 2}\right) \tag{18}$$

where N_a is Avogadro number (N=6.023 x 10^{23}). The value of electronic polarizability α can also be obtained using optical bandgap, which given as

$$\alpha = \left[1 - \frac{\sqrt{E_g}}{4.06}\right] \times \frac{M}{\rho} \times 0.396 \times 10^{-24} cm^3 \quad (19)$$

where E_g is the band gap (eV) of the crystal, and all these calculated parameters for the title crystal are listed in Table 6.

3.11. Z-scan measurements

The Z-scan technique is a highly sensitive and a useful tool for determining the magnitude and sign of nonlinear index of refraction (n_2) of solids, liquid solutions and thin films. The nonlinear absorption coefficient (β) of materials introduced by Sheik Bahae et al.[17, 18] It is widely accepted technique for the characterization of nonlinear optics by scientific community. In this experiment, the third-order NLO properties of the title crystal were investigated by using He–Ne laser (5mW) of wavelength at 632.8nm was used as a source and the beam diameter is 0.5 mm. It was focused with Gaussian filter to convert input laser beam into Gaussian form. The Gaussian beam TEM_{00} mode is passed through a convex lens with a focal length 30mm. This focal length completely depends on the incident Gaussian beam. The diameter of the Gaussian beam waist ω_0 at the focal length is 12.05μm. The sample is translated across in the +Z to -Z axial direction by the control of the stepper motor in order to vary the incident intensity falling on the crystal surface. The far filed transmittance intensity variations are measured through the closed aperture by using digital power meter (Field master GS-coherent). The recorded normalized transmittances in closed and open aperture curves for VSNS are given in Fig.18 and 19. From the closed aperture Z-scan curve, the pre-focal valley to post-focal peak configuration of the aperture curve suggests that the third order nonlinear refractive index change is positive. It is indicating a

self-focusing effect which is due to the reduced transmittance and large beam divergence through the far field aperture. An open aperture Z Scan data, the measurements were repeated the sample was moved along the focal point and without placing aperture in order to capture the entire transmitted beam by the detector. The essential criteria of sample thickness condition was satisfied for this measurement with the Rayleigh length (Z_R=K>L, where L denotes its thickness, and Z_R is the diffraction length of the Gaussian beam).[18] The value of Rayleigh length of a Gaussian laser beam can be calculated using the relation

$$Z_R = \frac{K\omega_0^2}{2} \tag{20}$$

where K is the wave vector ($K=2\pi/\lambda$ ($9.924x10^6$ m^{-1}) and ω_0 is the beam waist radius at the focal point given by

$$\omega_0 = \frac{f\lambda}{D} \tag{21}$$

where f is the focal length of the lens used, λ is the wavelength of the source and D is the beam radius at the lens. The difference between the transmittance change of peak and valley (ΔT_{p-v}) is evaluated by

$$\Delta T_{p-v} = 0.406(1-S)^{0.25}\left|\Delta\Phi_0\right| \tag{22}$$

where S is the aperture linear transmittance (S= 2) and r_a is the radius of the aperture and ω_a is the beam radius at the aperture. The linear transmittance and nonlinear refractive index (n_2) of the crystal was calculated by the using the relations.[53]

$$S = 1 - \exp\left(\frac{-2r_a^2}{\varepsilon_a^2}\right) \tag{23}$$

$$n_2 = \frac{\Delta\Phi_0}{KI_0L_{eff}} \tag{24}$$

where I_0 is the intensity of the laser beam at the focal point (I_0=26.50) and L_{eff} is an effective thickness of the crystal which can be calculated by using the relation $L_{eff} = [1-\exp(-\alpha L)]/\alpha$. Here, α is the linear absorption, and L is the thickness of the crystal. From the open aperture curve, the nonlinear absorption coefficient (β) can be determined using the following relation[17]

$$\beta = \frac{2\sqrt{2}\Delta T}{I_0L_{eff}} \tag{25}$$

where ΔT is the one valley value at the open aperture Z-scan curve. The value of β will be negative for saturated absorption and positive for two photon absorption processes.[54] The calculated values of n_2 and β was be used to determine the real and imaginary parts of the third-order nonlinear optical susceptibility can be obtained as

$$\mathrm{Re}\,\chi^{(3)}(\mathrm{esu}) = \frac{10^{-4}(\varepsilon_0 C^2 n_0^2 n_2)}{\pi}\left(\frac{\mathrm{cm}^2}{\mathrm{W}}\right) \tag{26}$$

$$\mathrm{Im}\chi^{(3)}(\mathrm{esu}) = \frac{10^{-2}(\varepsilon_0 C^2 n_0 \lambda\beta)}{4\pi^2}\left(\frac{\mathrm{cm}^2}{\mathrm{W}}\right) \tag{27}$$

where and ε_0 is the permittivity of free space (8.8518×10^{-12}F/m), n_0 is the linear refractive index of the crystal and C is the velocity of light in vacuum. The absolute value of the third-order nonlinear optical susceptibility $\chi^{(3)}$ is thus

$$\left|\chi^{(3)}\right| = \left[\left(\mathrm{Re}(\chi^{(3)})\right)^2 + \left(\mathrm{Im}(\chi^{(3)})\right)^2\right]^{1/2} \tag{28}$$

In addition, the second order hyperpolarizability γ which defines the nonlinear induced polarization per molecule, is related with the third order large susceptibility γ by.[55]

$$\mathrm{Re}[\gamma] = \frac{\mathrm{Re}\left[\chi^{(3)}\right]}{\mathrm{Nf}^4} \tag{29}$$

where N is the number of molecule per unit volume and the term f is the local field correction factor according to Lorentz expression is given by

$$f = \frac{(n_0^2 + 2)}{3} \tag{30}$$

The coupling factor $\rho = \mathrm{Im}((\chi^3)/\mathrm{Re}(\chi^3)$ is the ratio of the imaginary part ($\mathrm{Im}((\chi^3))$ to the real part ($\mathrm{Re}(\chi^3)$) of third order nonlinear susceptibility. The calculated coupling factor ρ is found to be 57.57. It is due to the contribution of nonlinear absorption change is more dominant than the nonlinear refraction and the electronic origin of nonlinearity.[56] According to eqs. (20)- (24), the third order nonlinear refractive index (closed-aperture) is (n_2, 5.214 m^2/w), the nonlinear absorption coefficient (open-aperture) (β, 5.954 m/W), the absolute value of third-order nonlinear susceptibility (χ^3, 6.564 x10 $^{-5}$esu) and the second order molecular hyperpolarizability (γ, 7.986 x10^{-34} esu) are calculated for VSNS crystal and are shown in Table 7. The larger value of second order molecular hyperpolarizability γ was mainly due to the higher π-electron conjugation present in the VSNS crystal. The open aperture Z-Scan curves exhibit the decrease in transmission with increase in the input intensity. Its indicating the presence of reverse saturable absorption (RSA) (excited state absorption) with a positive nonlinear absorption coefficient which leads to the material for optical limiting applications.[57,58] The reverse saturable absorption (RSA) refer to the absorption of the molecule in the excited state is high than the ground state.[59] Thus, the excellent nonlinear optical properties of the grown crystal are a promising material for optical limiting applications.

Conclusions

A new stilbazolium derivative crystal has been synthesized, and the single crystals were grown by slow evaporation method for the first time. Its crystal structure has been confirmed by single crystal x -ray diffraction analysis and showed the arrangement of molecule and formation of hydrogen bond in the grown crystal. The morphology of the grown crystal reveals that the prominent growth found to be the along the b -axis. The powder x- ray diffraction study confirms that the crystalline perfection is fairly good. The presence of functional groups and molecular structure of grown crystal was confirmed by FTIR and NMR spectral analysis. The Uv-Vis-NIR spectrum of the VSNS crystals shows that are highly transparent in nature in the Vis-NIR region and the cut-off wavelength is found to be 390nm. The calculated optical band gap value was found to be 3.252eV using Tauc's plot. The optical parameter such as the absorption coefficient (α), reflectance (R) refractive index (n_0), extinction coefficient (K), were calculated to analyze its optical properties. The transparency of the grown crystal is good and is quite for optoelectronic and NLO applications. Further, the photoluminescence shows green emission radiation. TG/DTA studies indicate that the compound is thermally stable up to its melting point 196.6 ^{o}C. The dielectric measurement of VSNS reveals the low dielectric constant and loss at higher frequencies and hence this crystal is more attractive for optoelectronic applications and NLO devices. The electronic polarizability (α) of the grown crystal has been calculated by Penn analysis using dielectric constant and which agrees with that of Clausius-Mossotti relation. The detailed study of Vickers hardness studies indicates that the material is suitable for nonlinear applications. The results of etching studies reveal the growth mechanism of title crystal layer pattern with minimum dislocations. The higher value of surface laser damage threshold of VSNS suggests that these crystals may have a favorable application in laser frequency conversion. The single beam Z-scan experimental results confirm the large

nonlinear absorption coefficient and positive value of third order nonlinear refractive index, which are most required for optical limiting applications. From the present investigation, we concluded that VSNS is a new candidate for the NLO device applications.

Acknowledgment

The authors are thankful to Defence Research and Development Organisation (DRDO), Government of India, for financial assistance (Project Ref. No. ERIP/ER/1103929M/01/1402). The authors are grateful to VIT University management for their constant support and the providing research facilities.

References

(1) C. Zhang, Y.L. Song, X. Wang, *Coord. Chem. Rev*. 2007, **251**, 111.

(2) P. N. Prasad, D. J. Williams, Introduction to Nonlinear Optical Effect in Molecules and Polymers, John Wiley & Sons, New York, 1991, 2–10.

(3) M. Spasenovi, M. Betz, L. Costa, H.M. Van Driel, *Phys. Rev.* 2008, **B 77,** 085201.

(4) D.S. Chemla, J. Zyss, Nonlinear Optical Properties of Organic Molecules and Crystals, vol. 1, Academic Press, London, 1987.

(5) J. Zyss, Molecular Nonlinear Optics: Materials Physics and Devices, Academic Press, New York, Physics and Devices, 1993.

(6) J. Badan, R. Hierle, A. Perigand, J. Zyss, In: and Williams, D.J. (Ed.). "Nonlinear Optical Properties of Organic Molecules and Polymeric Materials", 233 D. 5, American Chemical Society, Washington, DC, 1993.

(7) W. Denk, J.H. Strickler, W. W. Webb, *Science*.1990, **248**, 73–76.

(8) C. C. Corredor, Z. L. Huang, K.D. Belfield, A. R. Morales, M. V. Bondar, *Chem. Mater*.2007,**19***,* 5165–5173.

(9) C.Q. Tang, Q. Zheng, H. M. Zhu, L. X. Wang, S. C. Chen, E. Ma, X.Y. Chen, *J. Mater.Chem. C*. 2013*,* **1**, 1771–1780.

(10) M. Samoc, N. Gauthier, M. P. Cifuentes, F. Paul, C. Lapinte, M.G. Humphrey, *Angew. Chem. Int. Ed*. 2006, **45**, 7376.

(11) W. Guan, G.C. Yang, G. C. Liu, P. Song, L. Fang, L. K. Yan, Z. M. Su, *Inorg. Chem.*2008, **47**, 5245.

(12) Y. Takahashi, H. Adachi, T. Taniuchi, M. Takagi, Y. Hosokawa, S. Onzuka, S. Brahadeeswaran, M. Yoshimura, Y. Mori, H. Masuhara, T. Sasaki, H. J. Nakanishi, *Photochem Photobiol A.* 2006,**183**,247.

(13) B.J. Coe, J. A. Harris, I. Asselberghs, K. Wostyn, K. Clays, A. Persoons, B. S. Brunschwig, S. J. Coles, T. Gelbrich, M. E. Light, M.B. Hursthouse, K. Nakatani, *Adv. Funct. Mater.* 2003, **13**, 347.

(14) G. R. Meredith, In Nonlinear Optical Properties of Organic and Polymeric Materials; D.J. Williams, Ed.; ACS Symposium Series, **233**, American Chemical Society: Washington, DC, 1983, 27-56.

(15) G. Seetharam Shettigar, K. Umesh, Chandrasekharan, Balakrishna Kalluraya, *Synthetic Metals,* 2007, **57**, 142–146.

(16) J. H. Klein-Wiele, M. A. Bader, I. Bauer, S. Soria, P. Simon, G. Marowsky, *Synth.Met.* 2002, **127**, 53–57.

(17) M. Sheik-Bahae, A. A. Said, E. W. Van Stryland, *Opt. Lett*. 1989, **14**, 955-957.

(18) M. Sheik-Bahae, A.A. Said, T. H. Wei, D.J. Hagan, E.W. Van Stryland, *Journal of Quantum Electronics*, 1990, 760-769.

(19) M.G. Kuzyk, C. W. Dirk, *Marcel Dekker, Inc.*1998.

(20) W. S. Wang, K. Sutter, Bosshard, Ch, Z. Pan, H. Arend, P. Gunter, G. Chapuis, F. Nicolo, *Jpn .J. Appl. Phy*. 1988, **27**, 1138-1141.

(21) W. J. Kaminsky, *Appl. Cryst.* 2007, **40**, 382.

(22) G. M. Sheldrick, *Acta Cryst.*2008, **A64**, 112–122.

(23) G. Socrates, Infrared and Raman of Characteristic Frequencies, Third ed., John Wiley and Sons Ltd., Chichester, **2001**.

(24) V. Balachandran, K. Parimala, *Spectrochim acta. A*. 2012, **95**, 354–368.

(25) P. N. Prasad,Springer, Ser. Wave-Phenom., 1989, **9**, 305–327.

(26) D.D.O Eya, A. J. Ekpunobi, C.E. Okeke, *Acad. Open Internet J*. 2006, 17.

(27) S. Redrothu Hanumantharao, S. Kalainathan, G. Bhagavannarayana, U. Madhusoodanan, *Spectrochim acta. A*. 2013,**103**, 388–399.

(28) S. Sudhahar, M. Krishna Kumar, B. N. Sornamurthy, R. Mohan Kumar, *Spectrochim acta. A*. 2014, **118**, 929–937.

(29) B.R. Lawn, E.R. Fuller, *J. Mater. Sci*. 1975, **10**, 2016–2024.

(30) J. H. Westbrook, Flow in rock salt structure, Report 58-R L, 2033 of GE Research Laboratory, USA, 1958.

(31) C.C. Desai, J. L. Rai, *Bull. Mater. Sci.*1983, **5**, 453.

(32) K. K. Rao, D. B. Sirdeshmukh, *B mater sci*.1983, **5**, 449–452.

(33) K. Sangwal, *Mater. Chem. Phys*. 2000, **63,**145.

(34) R. Vijayan, R. Ramesh Babu, R. Gopalakrishnan, P. Ramasamy, W.T.A. Harrison, *J Cryst Growth*. 2004, **262**, 490–498.

(35) G. Prasad, T. Prasad, S. V. Bhimasankaran, G. S. Suryanarayan, Kumar. *Indian j pure ap phy*. 1996, **34**, 639.

(36) W.A.Wooster, *Rep prog phys*. 1953, **16**, 62-82.

(37) C. Hays, E. G. Kendall, *Metallography*. 1973, **6***,* 275.

(38) A. A. El-Fadl, A. S. Soltan, N. M. Shaalan, *Cryst. Res. Technol*. 2007, **42***,* 364–377.

(39) P. Pandi, G. Peramaiyan, M. Krishna Kumar, R. Mohan Kumar, R. Jayavel, R. *Spectrochim acta. A*. 2012, **88***,* 77-81.

(40) W. L. Smith, *Opt Eng*, 1959, **17**, 489.

(41) B. C. Stuart, M.D. Feit, A.M. Rubenchik, B.M. Shore, M. D. Perry, *Phy Rev Lett*. 1995, **74**, 2248.

(42) G.C. Bhar, A.K. Chaudhary, P. Kumbhakar, *App Surf Sci*, 2000; **161**,155-62.

(43) N. Vijayan, G. Bhagavannarayana, K.R. Ramesh, R. Gopalakrisnan, K.K. Maurya, P. Ramasamy, *Cryst. Growth Des*. 2006, **6**, 1542.

(44) H. M. Lin, Y. F. Chen, J. L. Shen, W.C. Chou, *J. Appl. Crystallogr*. 2001, **89**, 4476.

(45) J. Philip, T.A. Prasada Rao, *Phys Rev A*, 1992, **46**, 2163–2165.

(46) H.J. Coles, S.V. Kershaw, *J Chem Soc Perk T*. 1988, 987–996.

(47) B. B. Parekh, M. J. Joshi, Cryst. Res. Technol. 2007, **42 (2)**, 127–132.

(48) S. A. Mazen, F. Metawe, S.F. Mansour, *J. Phys. D: Appl. Phys*. 1997, **30**, 1799-1808.

(49) C. Balarew, R. Duhlew, *J. Solid State Chem.* 1984, **551**, 1–6.

(50) N. M. Ravindra, R. P. Bharadwaj, K. Sunil Kumar, V. K. Srivastava, *Infrared Phys.*1981, **21**,369.

(51) J. D. Jackson, *Classical Electrodynamics.* 1978*, 321(Wiley Eastern).*

(52) N. M. Ravindra, V.K. Srivastava, *Infrared Phys*. 1980, **20**, 67-69.

(53) E. M. Van Stryland, M. Sheik-Bahae, M. G. Kuzyk, C.W. Dirk, *Marcel Dekker Inc*. 1998, 655–692.

(54) T. C. Sabari Girisun, S. Dhanuskodi, D. Mangalaraj, Phillip. *J. Current Applied Physics* 2011, **11**, 838–43.

(55) M.T. Zhao, B.P. Singh, P. N. Prasad, *J. Chem. Phys*. 1998, **89**, 5535.

(56) K. Naseema, M. Shyma, K.B. Manjunatha, A. Muralidharan, G. Umesh, Vijayalakshmi Rao. *Opt laser technol*, 2011, **43***,* 1286–1291.

(57) J. Wang, W.J. Blau, *J. Opt. A: Pure. Appl. Opt.* 2009, **11**, 024001.

(58) F.Z. Henari, W. J. Balua, L. R. Milgrom, G. Yahyoglu, D. Philips, J.A. Lacey, *Chem Phys Lett*. 1997, **267**, 229.

(59) F.Z. Henari, *J Opt A: Pure Appl Opt*. 2001, **3**,188.

Caption of the Tables

Table 1

Crystal data and structure refinement for VSNS

Empirical formula	C_{25} H_{27} N O_7 S.	
Formula weight	485.54	
Temperature	298(2) K	
Wavelength	0.71073 Å	
Crystal system	Monoclinic	
Space group	P2(1)/n	
Unit cell dimensions	a = 16.9655(8) Å	α= 90°.
	b = 8.3200(4) Å	β= 106.275(2)°.
	c = 17.1232(8) Å	γ = 90°.
Volume	2320.14(19) $Å^3$	
Z	4	
Density (calculated)	1.390 Mg/m^3	
Absorption coefficient	0.187 mm^{-1}	
F(000)	1024	
Crystal size	0.25 x 0.20 x 0.15 mm^3	
Theta range for data collection	1.49 to 25.00°.	
Index ranges	-18<=h<=19, -8<=k<=9, -16<=l<=20	
Reflections collected	13898	
Independent reflections	3860 [R(int) = 0.0176]	
Completeness to theta = 25.00°	94.4 %	
Absorption correction	None	
Max. and min. transmission	0.9725 and 0.9548	
Refinement method	Full-matrix least-squares on F^2	
Data / restraints / parameters	3860 / 0 / 329	
Goodness-of-fit on F^2	1.047	
Final R indices [I>2sigma(I)]	R1 = 0.0331, wR2 = 0.0832	
R indices (all data)	R1 = 0.0389, wR2 = 0.0887	
Largest diff. peak and hole	0.249 and -0.349 $e.Å^{-3}$	

Table 2 Hydrogen bonds for VSNS [Å and deg].

D-H...A	d(D-H)	d(H...A)	d(D...A)	<(DHA)
O(6)-H(2OA)...O(4)#1	0.82(3)	2.03(3)	2.835(2)	164(3)
O(6)-H(2OA)...S(1)#1	0.82(3)	2.87(3)	3.6196(16)	152(2)
O(6)-H(1OA)...O(3)#2	0.87(3)	1.89(3)	2.730(2)	161(2)
O(7)-H(3OA)...O(5)#3	0.75(3)	2.04(3)	2.785(2)	170(2)
O(7)-H(3OA)...S(1)#3	0.75(3)	2.97(3)	3.677(2)	157(2)
O(7)-H(4OA)...O(6)#4	0.86(3)	1.86(3)	2.714(2)	177(3)
O(1)-H(5OA)...O(7)#5	0.86(2)	1.77(2)	2.638(2)	179(2)

Table 3 Bond length and angles for VSNS

Atoms	Length	Atoms	Angles
C(1)-N(1)	1.350(2)	N(1)-C(1)-C(2)	121.42(16)
C(2)-C(3)	1.381(3)	C(4)-C(3)-C(2)	119.31(18)
C(3)-C(4)	1.370(2)	C(3)-C(4)-C(5)	121.51(17)
C(4)-C(5)	1.390(2)	N(1)-C(5)-C(4)	117.04(14)
C(5)-N(1)	1.369(2)	N(1)-C(5)-C(6)	119.04(14)
C(5)-C(6)	1.449(2)	C(4)-C(5)-C(6)	123.91(15)
C(6)-C(7)	1.331(2)	C(7)-C(6)-C(5)	123.61(16)
C(7)-C(8)	1.455(2)	C(13)-C(8)-C(9)	118.03(14)
C(8)-C(13)	1.385(2)	C(13)-C(8)-C(7)	123.53(14)
C(8)-C(9)	1.401(2)	C(9)-C(8)-C(7)	118.44(15)
C(12)-C(13)	1.378(2)	C(10)-C(9)-C(8)	121.58(15)
C(14)-N(1)	1.474(2)	O(1)-C(10)-C(11)	117.09(14)
C(15)-O(2)	1.413(2)	C(13)-C(12)-C(11)	120.62(16)
C(16)-C(17)	1.364(2)	C(12)-C(13)-C(8)	120.88(15)
C(16)-C(25)	1.407(2)	C(17)-C(16)-C(25)	120.88(15)
C(17)-C(18)	1.414(2)	C(16)-C(17)-C(18)	120.22(15)
C(18)-C(19)	1.416(2)	C(17)-C(18)-C(19)	122.48(16)
C(18)-C(23)	1.417(2)	C(17)-C(18)-C(23)	118.84(15)
C(19)-C(20)	1.361(3)	C(20)-C(19)-C(18)	120.49(19)
C(20)-C(21)	1.395(3)	C(19)-C(20)-C(21)	120.72(19)
C(21)-C(22)	1.356(3)	C(22)-C(21)-C(20)	120.40(18)
C(22)-C(23)	1.413(2)	C(24)-C(23)-C(22)	121.99(16)
C(23)-C(24)	1.411(2)	C(24)-C(23)-C(18)	119.21(15)

Table 4 Microhardness, Yield strength and elastic stiffness constant values of VSNS.

Load P (g)	H_v (kg/mm^2)	σ_y (GN/m^2)	C_{11} x 10^{15} Pa
10	38.51	42.23	1.0217
25	52.20	57.26	1.7403
50	82.42	90.40	3.8701
100	125.83	138.01	8.1140

Table 5 Results of constant W, A_1 and H_o for VSNS

Hays–Kendall approach	Results
Resistance pressure (W)	-9.15 (g)
Load independent constant (A_1)	0.0480 (g/μm^2)
Corrected hardness (H_o)	89 (g/μm^2)

Table 6 Electric property for the grown VSNS crystal.

Parameters	**Values**
Plasma energy (eV)	20.67
Penn gap (eV)	0.7731
Fermi energy (eV)	16.72
Eelectronic polarizability (α) using Penn analysis	13.77 x 10^{-23} cm^3
Eelectronic polarizability (α) using Clausiuse Mosotti equation	13.79 x 10^{-23} cm^3
Eelectronic polarizability (α) using Optical band gap	7.68 x 10^{-23} cm^3

Table 7 Obtained Non-linear optical parameter from Open- and closed-aperture Z- scan measurement data for VSNS crystal

Laser beam wavelength (λ)	632.8nm
Lens focal length (f)	30mm
Optical bath length	85cm
Beam radius of the aperture (w_a)	3.5mm
Aperture radius (r_a)	1mm
Sample thickness (L)	0.63mm
Effective thickness (L_{eff})	2.040×10^{-3}m
Linear absorption coefficient (α)	-3207
Nonlinear refractive index (n_2)	5.214×10^{-12} m^2/W
Nonlinear absorption coefficient (β)	5.954×10^{-5} m/W
Real part of the third-order susceptibility [Re(χ^3)]	1.140×10^{-6} esu
Imaginary part of the third-order susceptibility [Im((χ^3)]	6.564×10^{-5} esu
Third-order nonlinear optical susceptibility (χ^3)	6.564×10^{-5} esu
Second-order molecular hyperpolarizability (γ)	7.986×10^{-34} esu

Scheme 1. Synthesis of VSNS

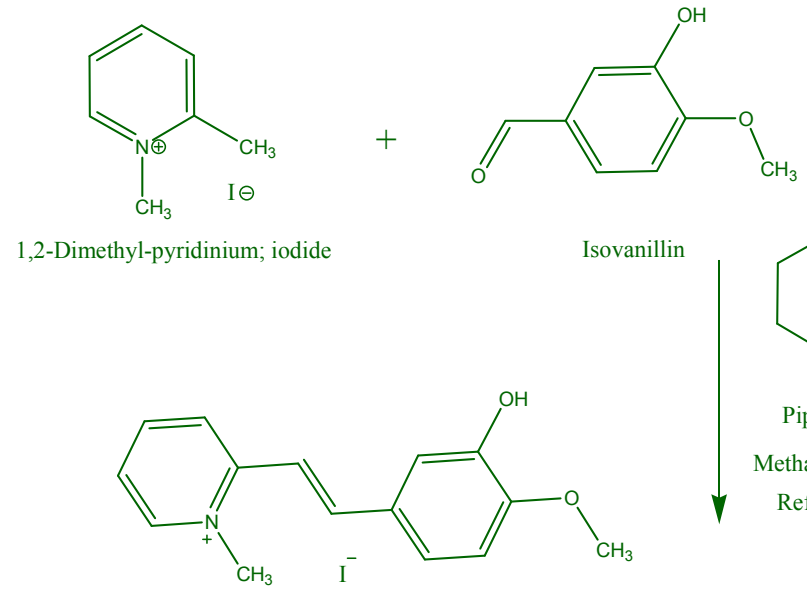

Caption of the Figures

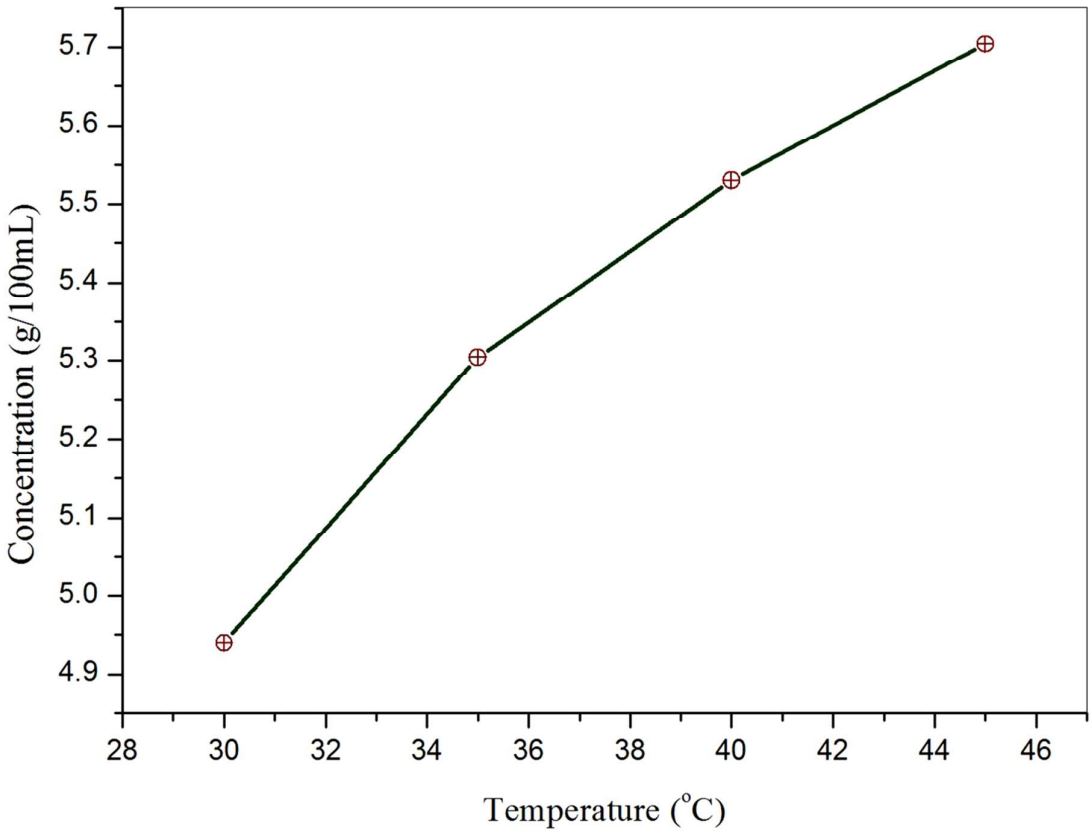

Fig 1. Solubility curve of VSNS as a function of temperature

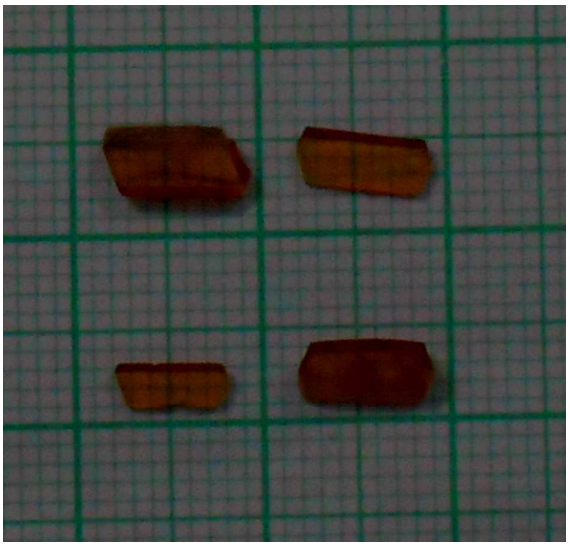

Fig. 2 Photograph of VSNS crystal grown by slow evaporation.

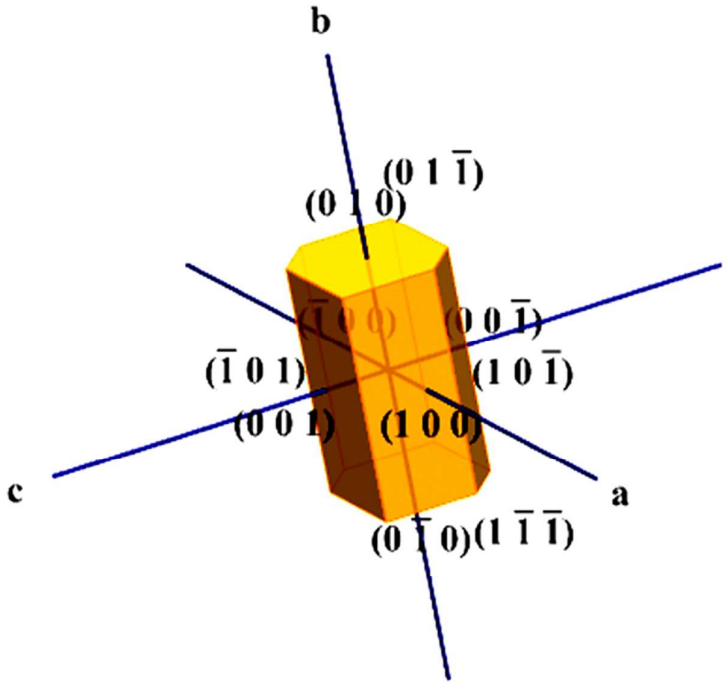

Fig. 3 Morphology of VSNS crystal.

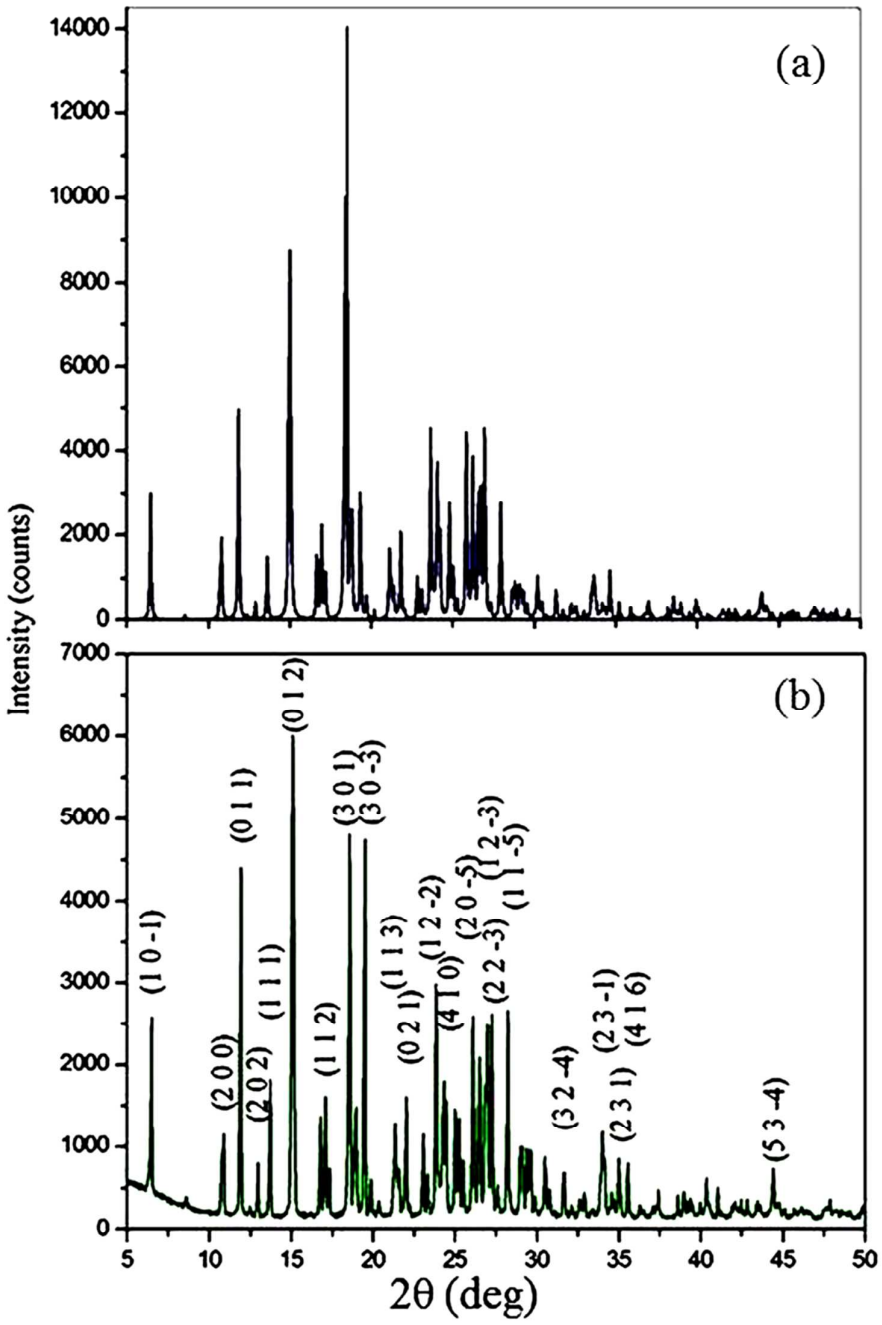

Fig. 4 Powder XRD patterns of VSNS: (a) simulated and (b) experimental.

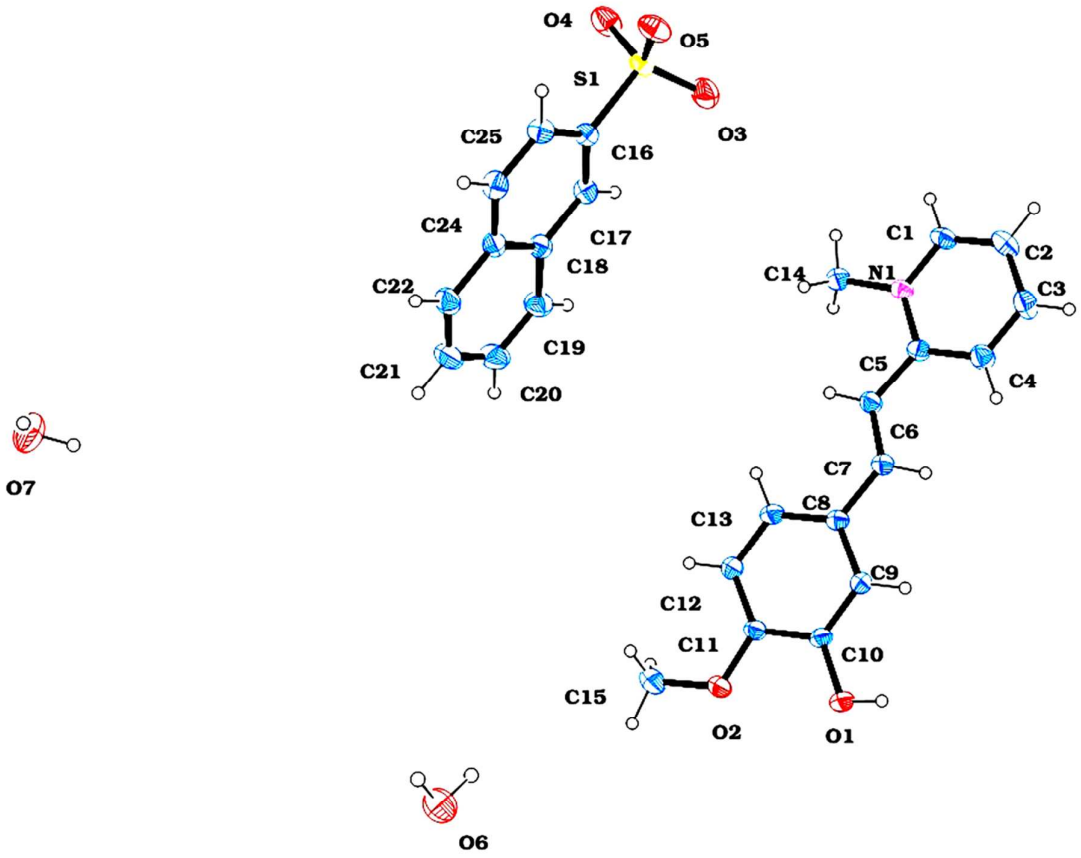

Fig. 5 ORTEP view of VSNS

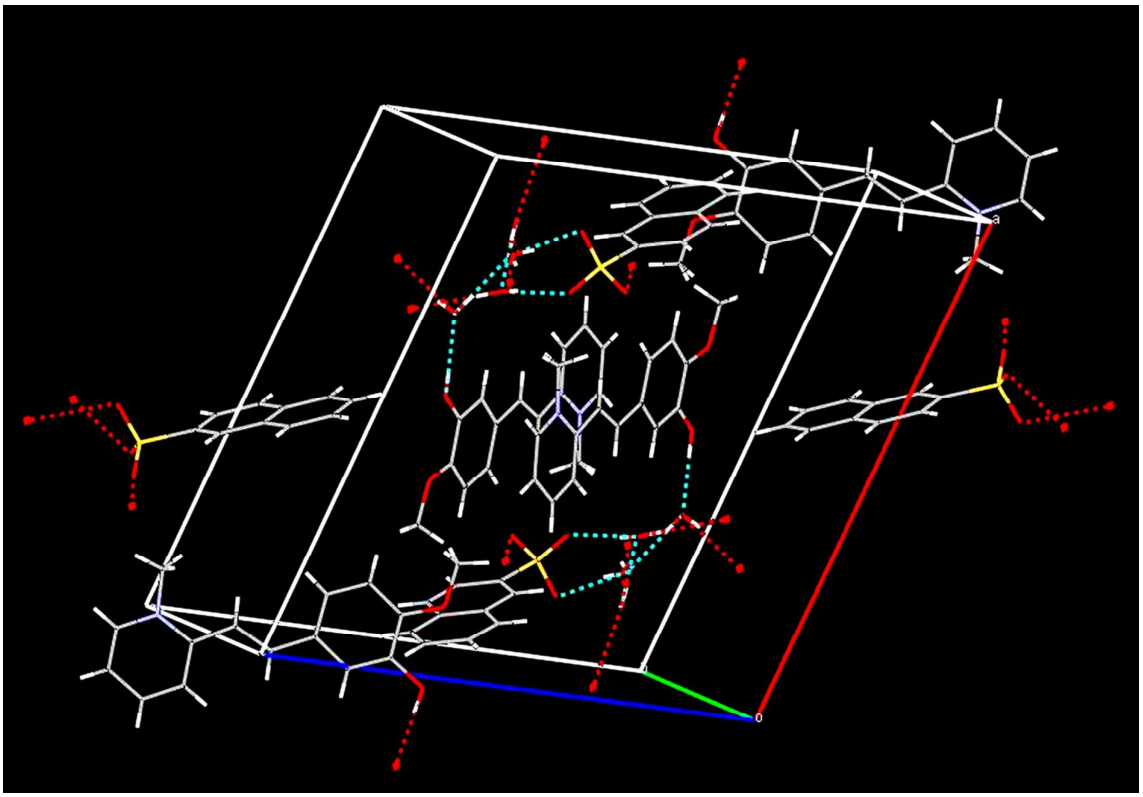

Fig. 6 Molecular packing diagram of VSNS

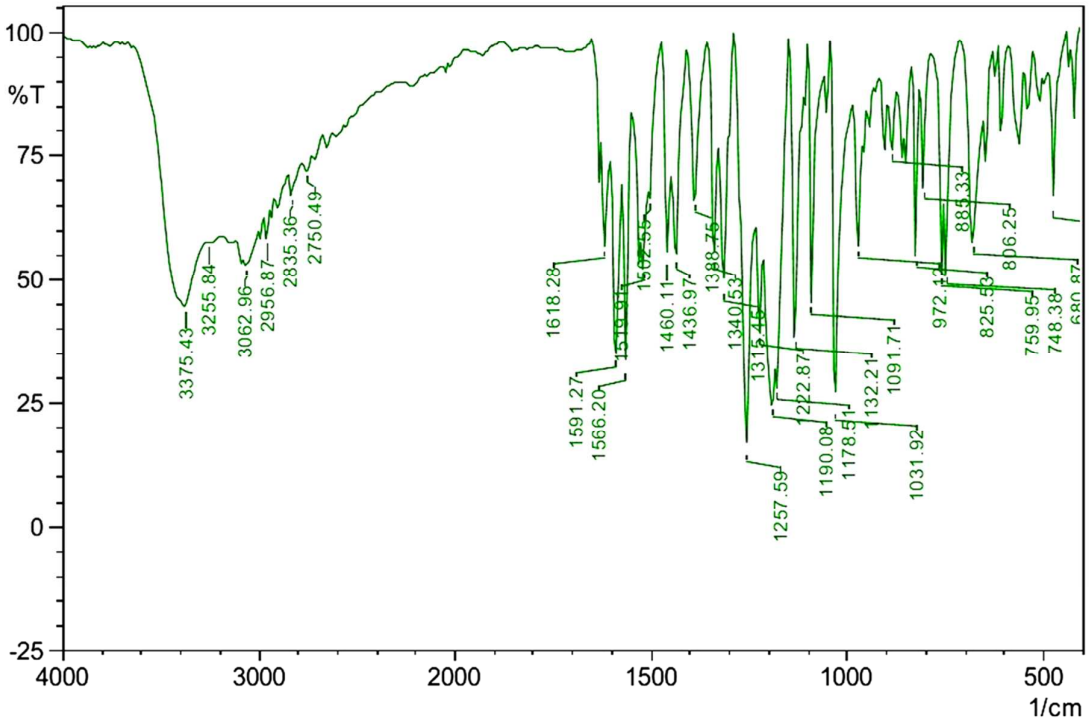

Fig. 7 FT-IR spectrum of VSNS

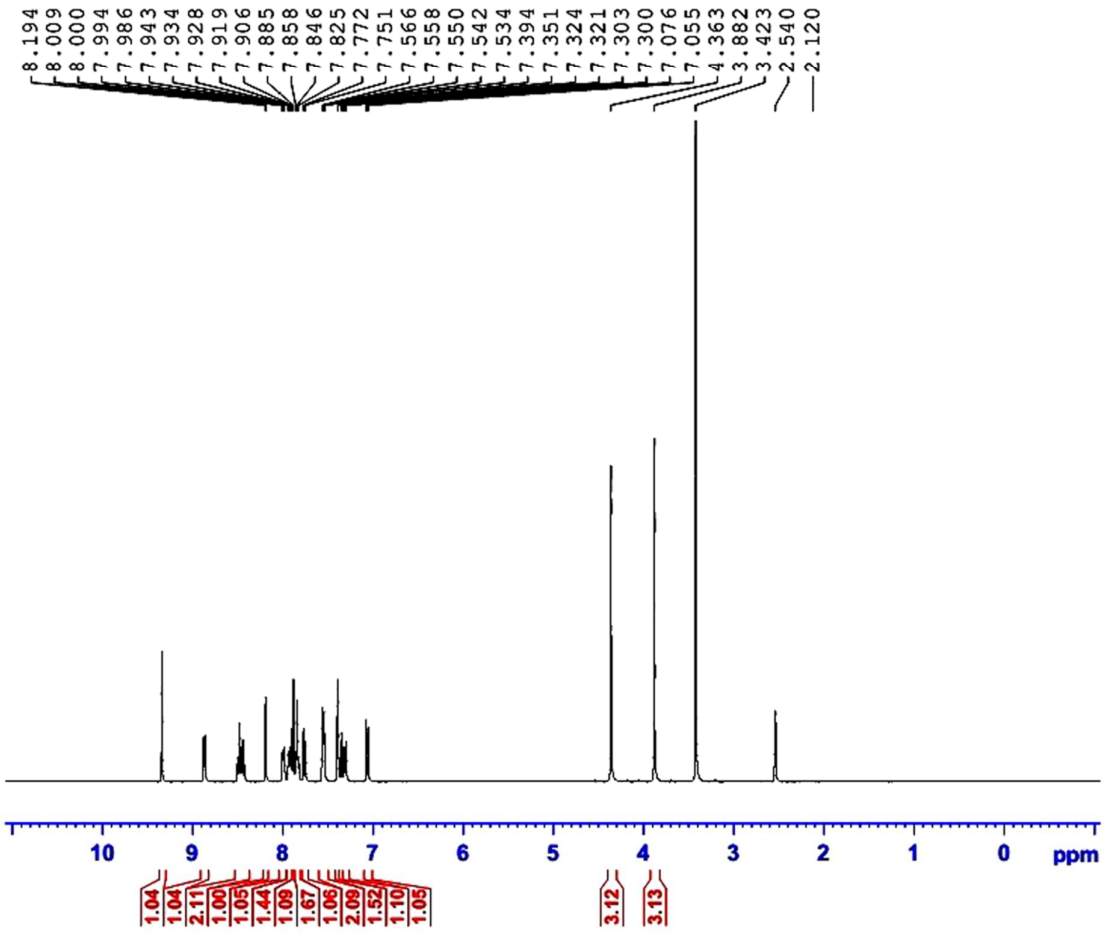

Fig. 8 ^{1}H NMR spectrum of VSNS

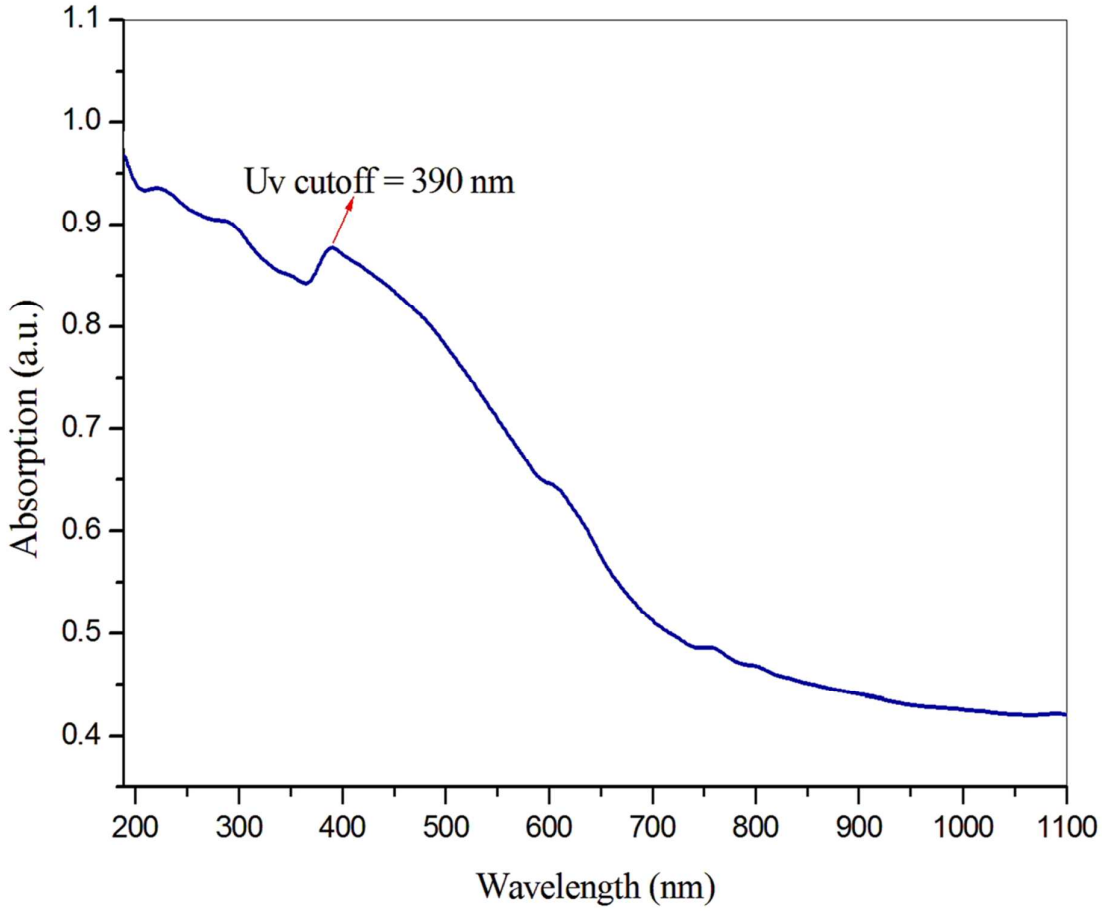

Fig. 9 UV–Vis NIR spectrum of VSNS

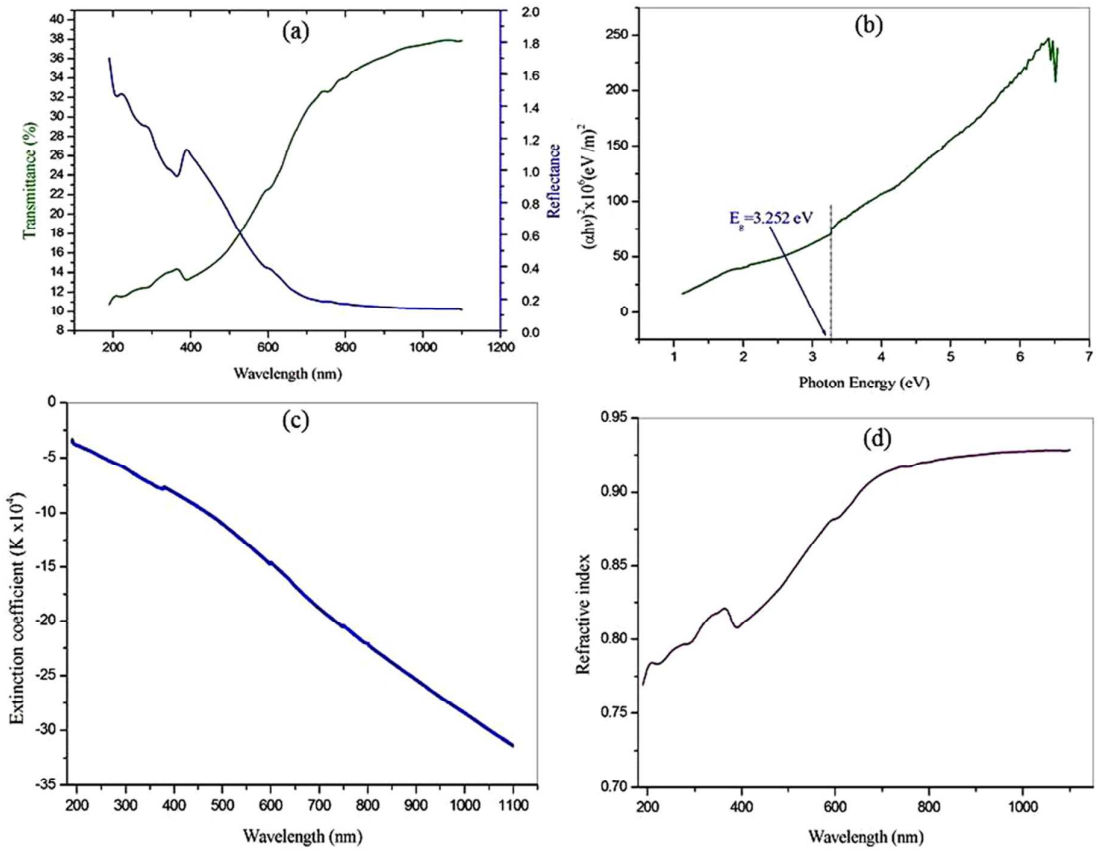

Fig. 10 The plot of transmittance and reflectance for VSNS (a), Plot of $(\alpha h\upsilon)^2$ against the photon energy ($h\upsilon$) (b), Wavelength dependence of extinction coefficient (K) (c), and refractive index (n_0) (d).

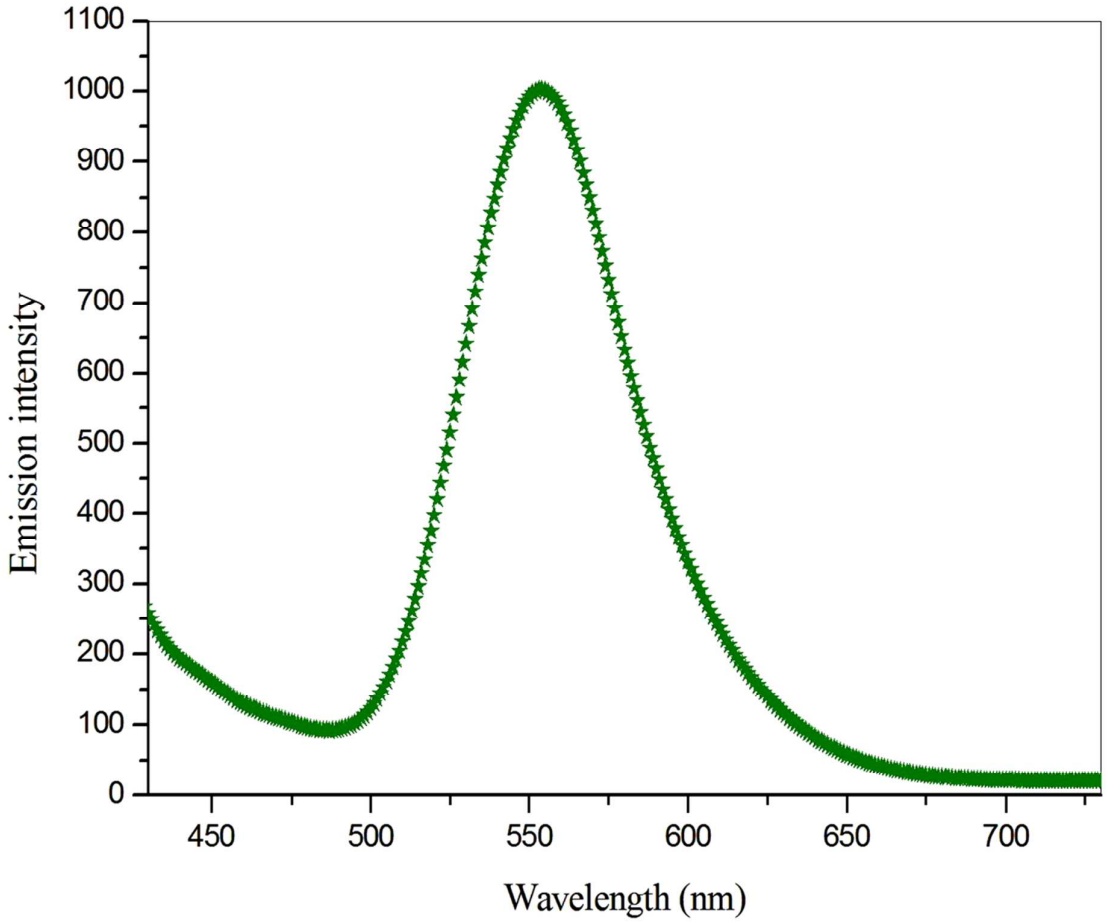

Fig.11 Emission spectra of VSNS

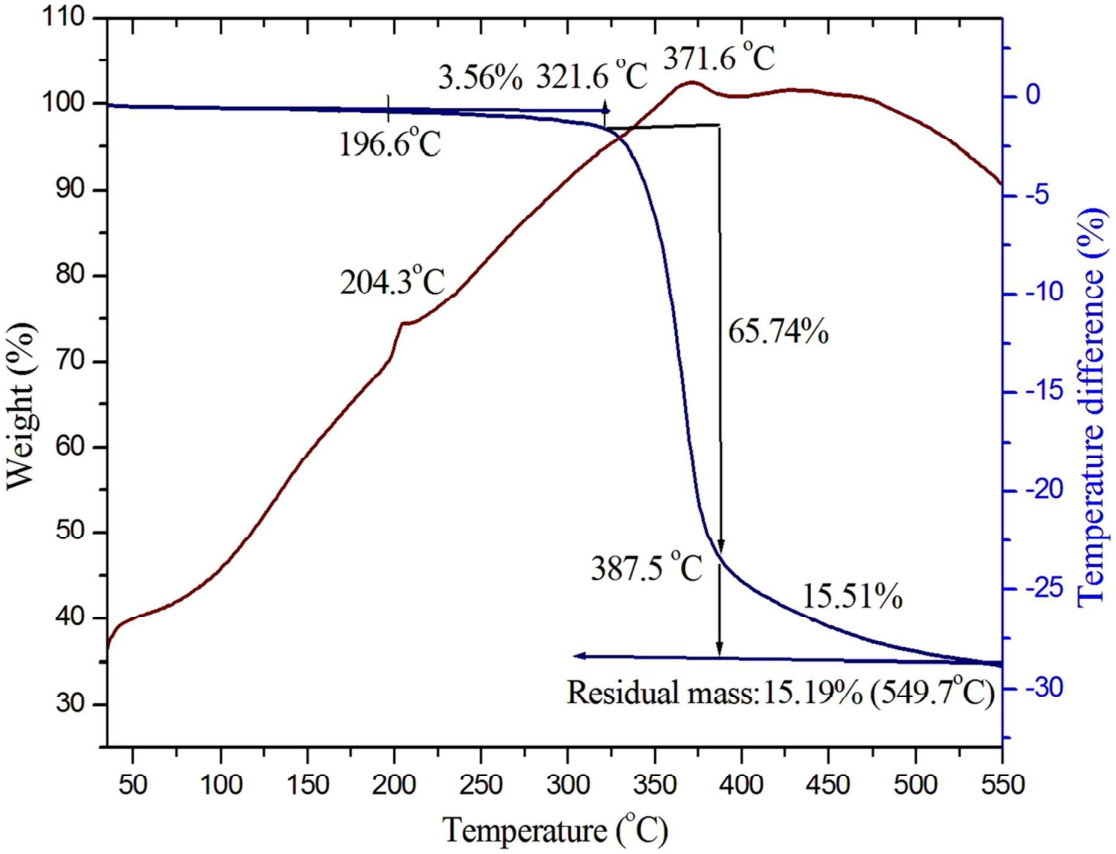

Fig. 12 TG/DTA curves of VSNS

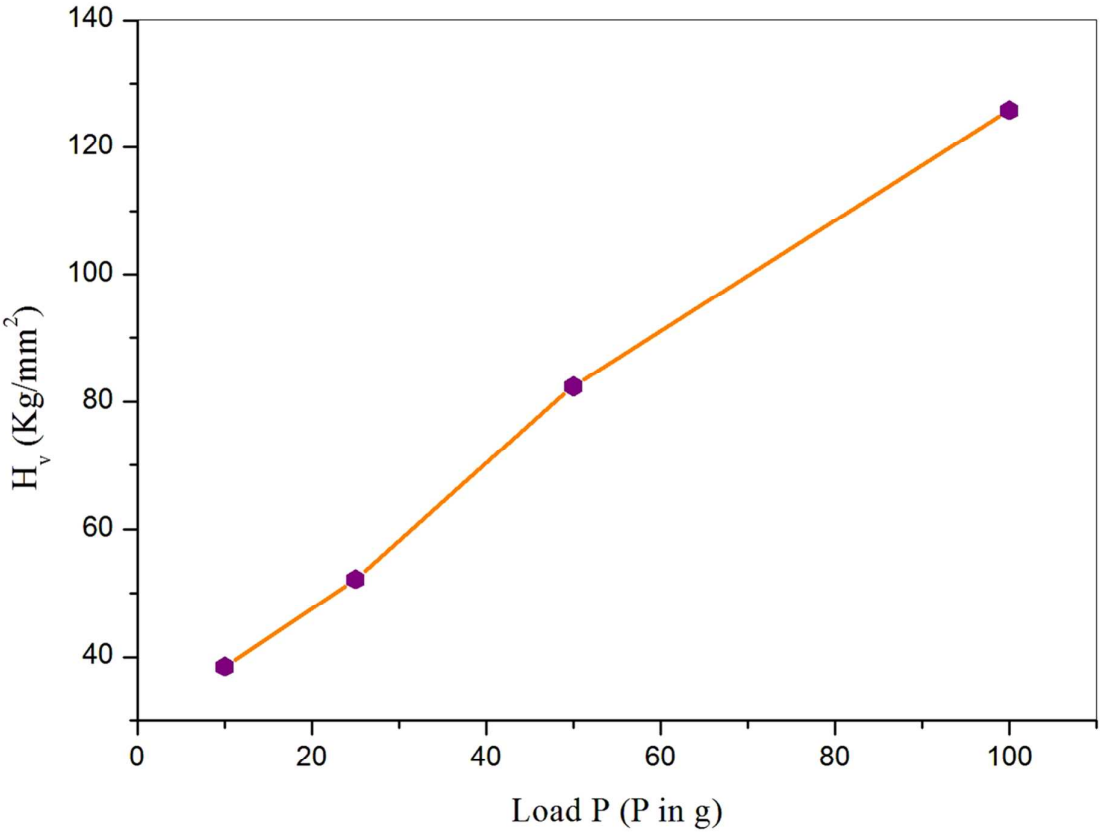

Fig.13 Variation of Hv with applied load P.

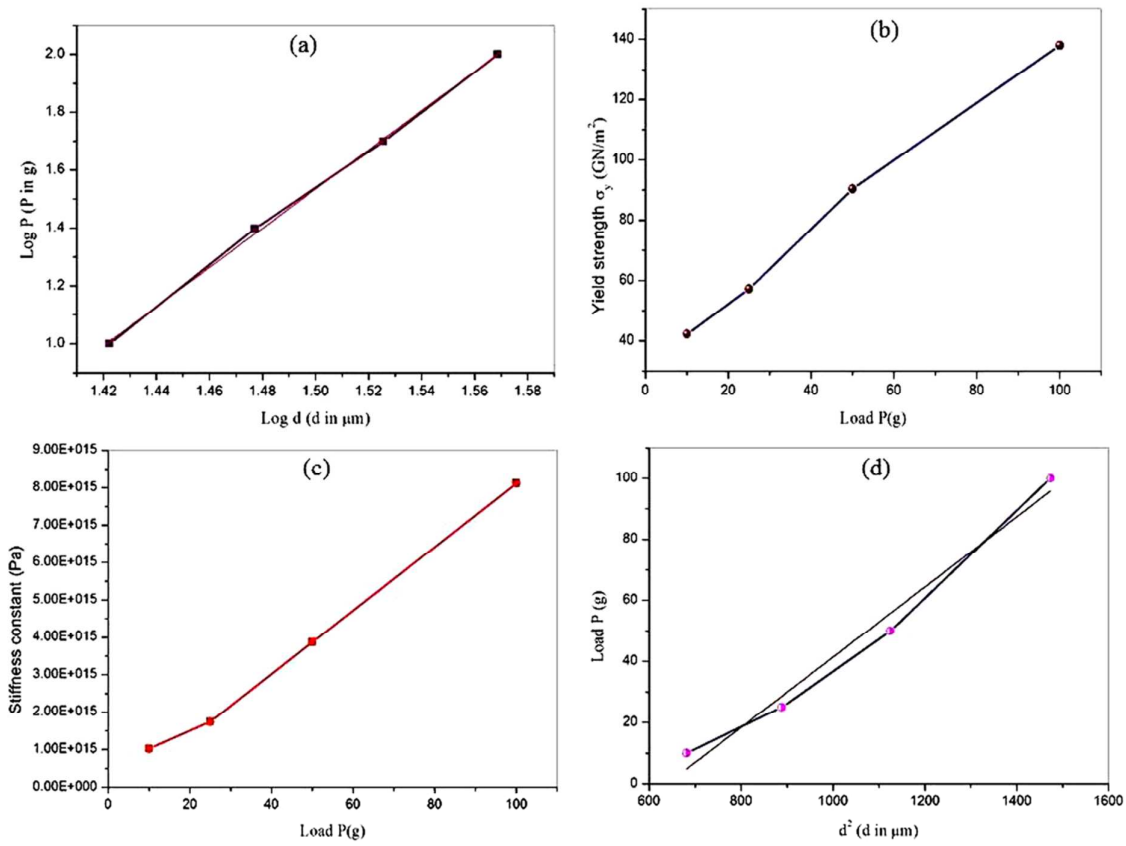

Fig. 14 Meyer's plot (a), Plot of yield strength vs. load (b), Variation of stiffness constant with load P (c), and Plot of load P vs. d^2 (d).

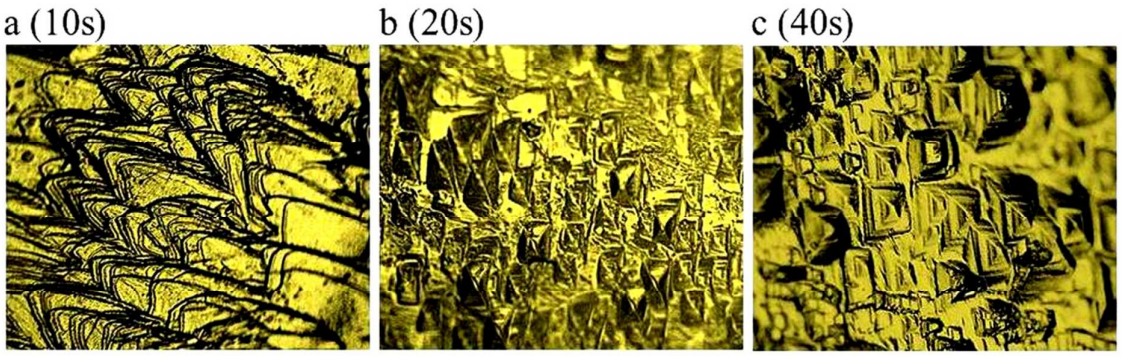

Fig. 15 Chemical etching time of VSNS single crystal on (1 0 0) face with methanol solvent as an etchant (a) as grown crystal surface, (b) 20 s, (c)10 s and (d)40 s.

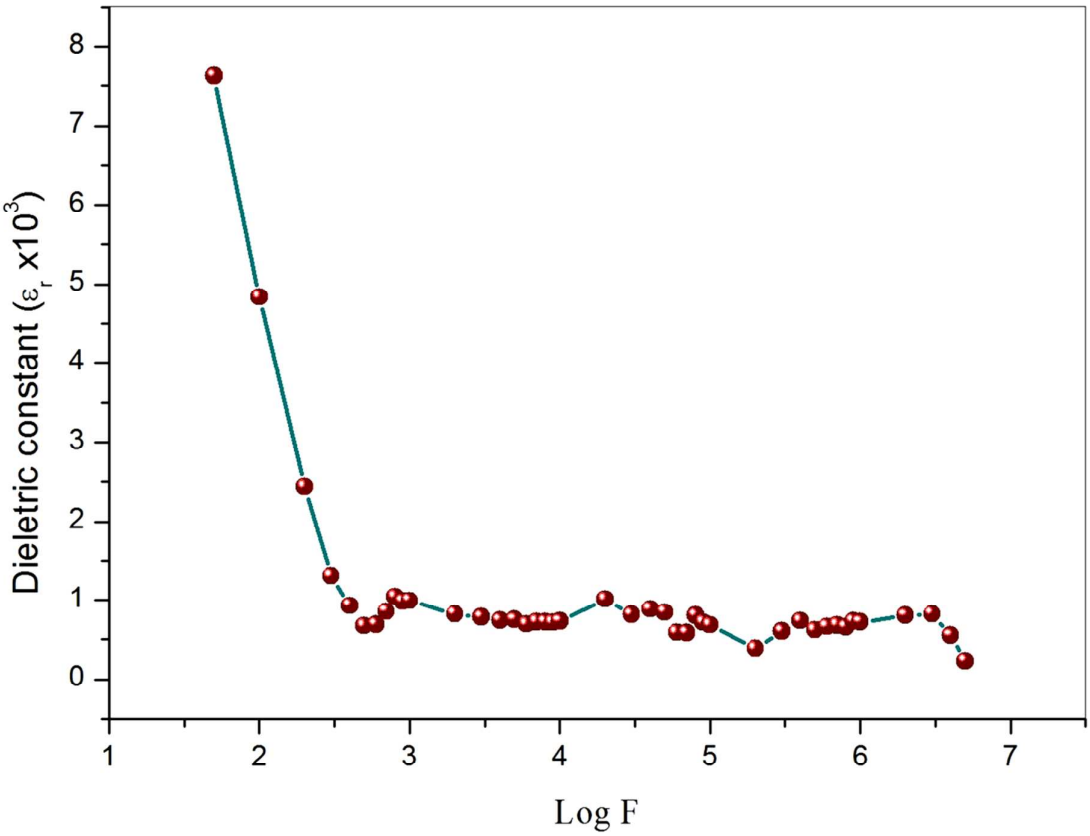

Fig. 16 Variation of dielectric constant with log frequency at room temperatures for VSNS single crystal.

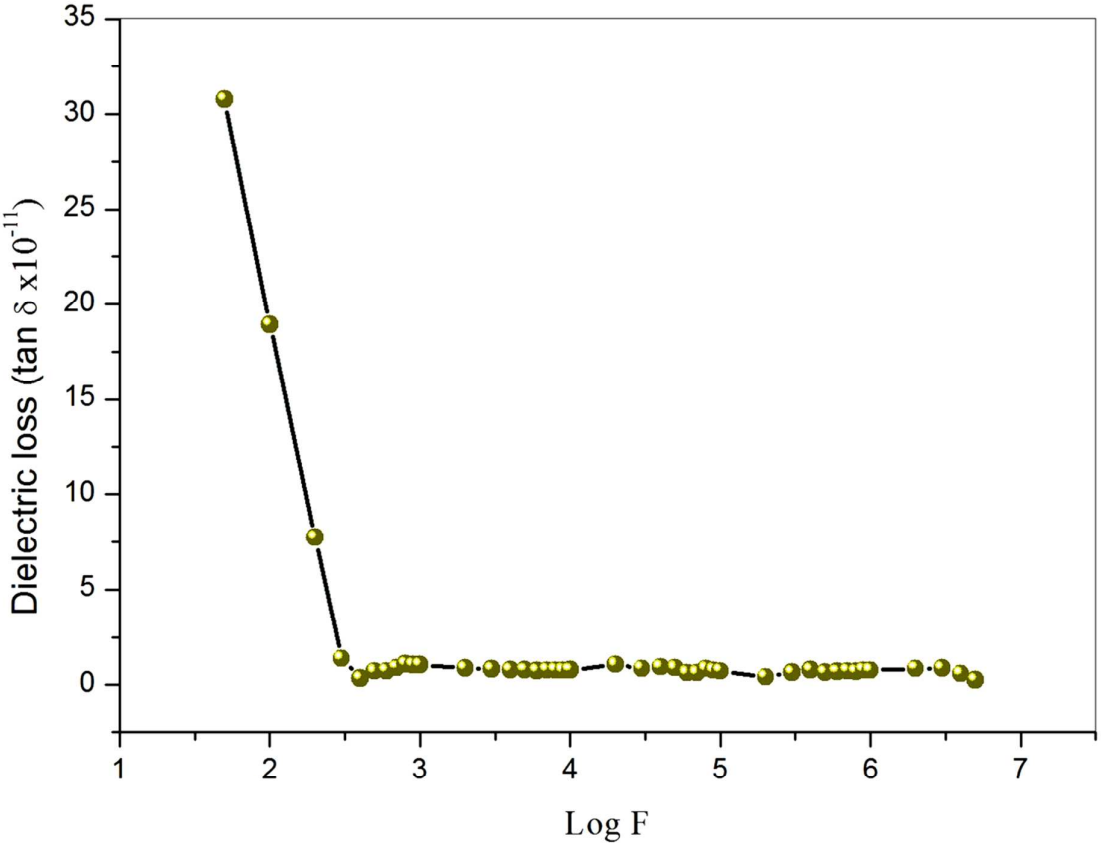

Fig. 17 Variation of dielectric loss with log frequency at room temperatures for VSNS single crystal.

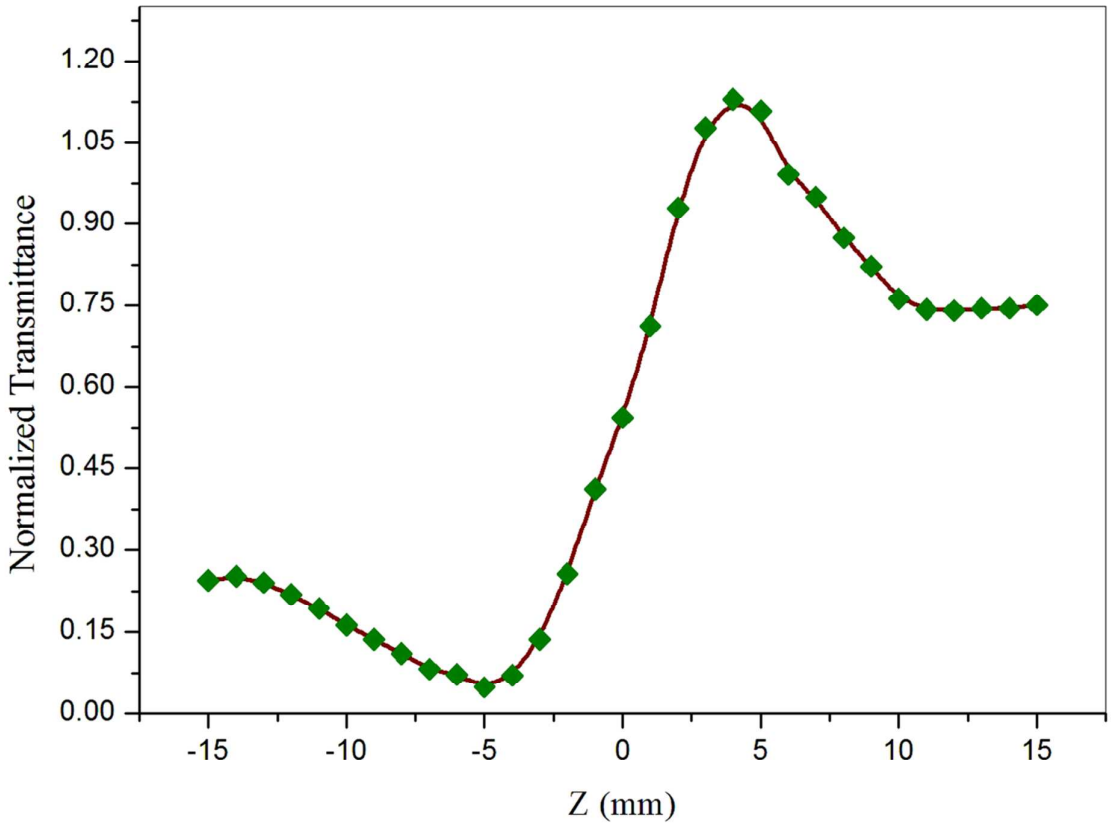

Fig. 18 Self-focusing (Closed aperture) Z-scan plot of VSNS crystal.

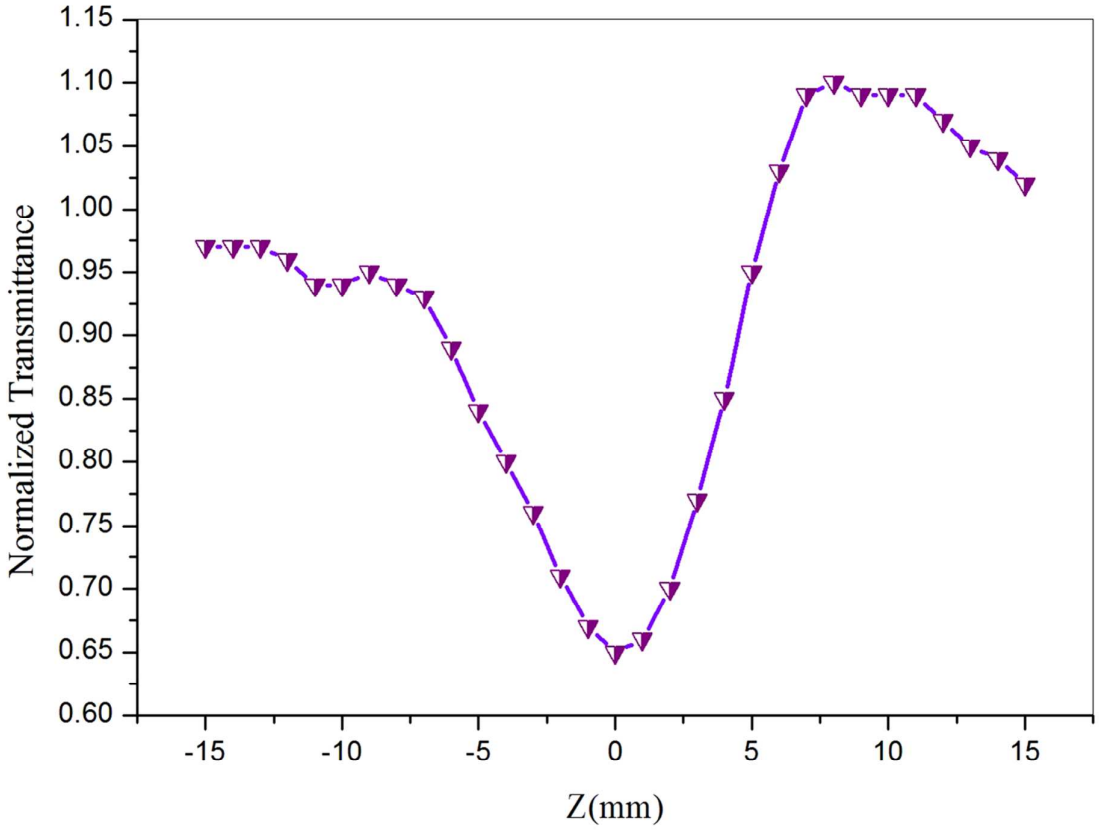

Fig. 19 Open aperture mode Z-scan plot of VSNS crystal.